Oligocene-early Miocene paradox of pCO_2 inferred from alkenone carbon isotopic fractionation and sea surface temperature trends

José Guitián^{1*}, Samuel Phelps^{2, 3}, Reto S. Wijker¹, Pratigya J Polissar^{2, 4}, Laura Arnold¹, and Heather M. Stoll¹

- 5 ¹Geological Institute, ETH Zurich, Switzerland
 - ²Lamont-Doherty Earth Observatory, Columbia University, USA
 - ³Harvard University, USA
 - ⁴Ocean Sciences Department, University of California Santa Cruz, USA
 - * present address: Centro de Investigación Mariña, Universidade de Vigo, GEOMA, Vigo, 36310, Spain
- 10 Correspondence to: Jose Guitian (jose.guitian@uvigo.gal; heather.stoll@eaps.ethz.ch)

Abstract. Atmospheric carbon dioxide decline is hypothesized to drive the progressive cooling over the Cenozoic. However, the long term CO₂ record from the early Oligocene to Miocene time interval, derived from the phytoplankton carbon isotopic fractionation (ε_p) proxy, differs from what is expected to drive the climate observations. Here, we produce two new long-term records of ε_p over the Oligocene to early Miocene time interval from widely separated locations at IODP Site 1406 and ODP 1168 and increase the resolution of determinations at the equatorial Atlantic ODP 925. These new results confirm a global trendfootprint of ε_p declineshift occurring during this interval. Rapid 3 % declines are found from 27 to 24.5 million years ago (Ma) and 24 to 22.5 Ma, and minimum ε_p is attained at 19 Ma. Between 29.728.7 and 29.728.7 -Ma at IODP 1406, a 20-30 ky sampling resolution at Site 1406 reveals orbital scale 100 kyr cyclicity in ε_p . Making use of alkenone-based sea surface temperature (SST) estimates and benthic δ^{18} O estimates extracted from the same samples, we perform a direct comparison with ε_p to evaluate the relationship with climate. We observe that across the long Oligocene to early Miocene interval, ε_p is 20 positively correlated to SST only at the Ssouthern Ocean Site 1168, but not with SST at the North Atlantic Site 1406. Accounting for the temperature-driven growth rate or cell size effects on ε_p does not lead to stronger correlations between ε_p and benthic δ^{18} O nor stronger correlations between ϵ_p and SST at Site 1406.- Moreover, at orbital timescale, the relationship between ε_p and benthic δ¹⁸O, albeit weak, implies greater ice volume or colder deep ocean at higher CO₂. Despite the persistence of climate paradox, the reproducible albeit trends in three widely separated sites, which experienced contrasting temperature evolution and likely experienced different variations in nutrient availability, suggest that a common CO2 forcing is likely the dominant control on the long term trends in ε_p . Changing ocean heat transport to the North Atlantic may contribute to the observed decoupling of long term ε_p Ep- and SST in this location. Atmospheric carbon dioxide decline is hypothesized to drive the progressive cooling over the Cenozoic. However, at multimillion year timescales during the Oligocene to Miocene time interval the existing reconstructions, most based on the phytoplankton carbon isotopic fractionation (ε_n) proxy, differ from what is expected to drive the climate observations. Here, we produce two new long-term records of s_p over the Oligocene to early Miocene time interval from widely separated locations at IODP Site 1406 and ODP 1168 and increase the resolution of determinations at the equatorial Atlantic ODP 925. These new results confirm a global footprint of s₀ shift occurring during this interval. Abrupt 3 % declines are found from 27 to 24.5 Ma and 24 to 22.5 Ma, and minimum ε_p is attained at 19 Ma. Between 28.7 and 29.7 Ma at IODP 1406, a higher resolution sampling reveals orbital scale 100 kyr cyclicity in Ep. Making use of alkenone-based sea surface temperature (SST) estimates and benthic δ^{48} O estimated extracted from the same samples, we perform a direct comparison with ϵ_p to evaluate the relationship with climate dynamics. We observe that across the long Oligocene to early Miocene interval the two sites' relationships contrast with what is expected if CO₂ was the main driver of ε_p and average earth surface temperature evolution was registered at the local surface SST and global benthic δ¹⁸O. Moreover, at orbital timescale, ε_p and benthic δ¹⁸O appear to follow an inverse relationship, although located within the multimillion year period with the strongest direct correlation between these variables (>25.5 Ma). To evaluate the physiological, non-CO₂-influences on ε_p, we use modern cultures to evaluate the impact of changing cell size and growth rate on the trends in ε_p. Although at specific time intervals, those drivers seem to explain part of the ε_p divergence with SST or benthic δ¹⁸O, most periods remain largely divergent, particularly the late Oligocene warming. We infer that a common CO₂-forcing is likely the dominant control on the coherent temporal trends in ε_p at widely separated sites, which experienced contrasting temperature evolution and likely experienced different variations in nutrient availability. While CO₂ changes likely caused significant changes in radiative forcing, SST variation at the examined sites may have been conditioned by regional heat transport, and the relationship between benthic δ¹⁸O and ε_p could reflect variable phasing between ice growth and global temperature.

Short summary. We reconstructed from sediments of different ocean sites phytoplankton carbon isotopic fractionation (ε_p), mainly linked to CO₂ variations, during the Oligocene to early Miocene. Records Data confirm long-term CO₂ record trends but show contrasting relationships with the sea surface temperatures evolution. We evaluate the role of non-CO₂ physiological factors such as temperature and nutrients at each site ε_p , highlighting the complexity of interpreting climate dynamics and CO₂ reconstructions.

1 Introduction

50

55

60

65

75

1.1 Oligocene to Miocene long term CO₂ and climate trends

Geological records provide key context to current assessments of the consequences of rising atmospheric CO₂ on ice sheet stability and oceanic temperatures (Foster et al., 2017; Golledge, 2020; Zachos et al., 2008). The Oligocene to Miocene time interval has been proposed to represent a nonlinear transition between the 'greenhouse' and 'icehouse' stages of Earth history (Miller et al., 1991; Zachos et al., 2001) useful to evaluate the Earth system climate sensitivity to the hypothesized progressive CO₂ drawdown of the Cenozoic (Deconto et al., 2008; Zhang et al., 2013). However, the long term decline in CO₂ estimated by existing proxy records contrasts with the rather stable climatic state with multimillion year warming- (e.g. Late Oligocene Warming) and cooling (e.g. Mi-1 glaciation) trends defined by the temperature trends in the interpreted from deep ocean (Cramer et al., 2011; Lear et al., 2000), and surface ocean records (Guitián et al., 2019; Liu et al., 2009; O'Brien et al., 2020) and with estimated Antarctic Ice sheet volume and sea level (Lear et al., 2004; Liebrand et al., 2017; Miller et al., 2020). The long term pCO₂ trends from the Oligocene to early Miocene are derived from the sensitivity of marine algae to pCO₂ based on the carbon isotopic fractionation in organic matter during photosynthesis (ε_p) of marine phytoplankton (Rau et al., 1996) Most of the Oligocene and early Miocene pCO₂ estimates are derived from the sensitivity of marine algae to CO₂ (Henderiks and Pagani, 2008; Pagani et al., 1999, 2000; Pagani et al., 2005; Super et al., 2018; Zhang et al., 2013) while published δ^{11} B based CO₂ estimates cover the latest Oligocene into early Miocene (younger than 24 Ma)based on the carbon isotopic fractionation in organic matter during photosynthesis (Ep) of marine phytoplankton (Rau et al., 1996), typically measured in biomarkers from haptophyte algae. This The algae isotopic fractionation can be reconstructed in the past from sediments by the analysis of δ^{13} C of the organic lipids and reconstruction of the δ^{13} C of the DIC in the seawater from which biomass was produced. Fractionation (ε_p) is predicted to be higher when CO_2 availability is high relative to cellular carbon demand. A decrease in atmospheric CO₂ and consequently in CO₂ of the surface ocean should therefore lead to a decrease in ε_p globally at any given site. However, in addition to CO₂, the ε_p in phytoplankton is affected by physiological factors such as the rate of carbon fixation, which may vary over time in a given location due to variations in temperature or the supply of light (Rau et al., 1996; Stoll et al., 2019).

One approach to evaluate the relative contribution of physiological factors vs CO₂ is to produce ε_p records from sites of widely contrasting oceanographic setting, where the CO₂ signal may be expected to be common to both locations but the environmental factors such as nutrient availability might not be expected to change in unison. The existing ε_p -based CO₂ estimations for the Oligocene are derived from ~1 million year.y. resolution measurements from two sites on the south American margin of the equatorial and South Atlantic; in the early Miocene an additional North Atlantic record provides data (CenCO2PIP Consortium, 2023). In this study, we produce a new long-term record of ε_p over the Oligocene to Miocene time interval at two new, widely separated locations: IODP Site 1406 in the subtropical mid latitude North Atlantic off the Newfoundland coast, and ODP 1168 in the Southern Ocean off of Tasmania. One approach to evaluate the relative contribution of physiological factors vs CO₂ is to produce ε_p records from sites of widely contrasting oceanographic setting, where the CO₂ signal may be expected to be common to both locations but the environmental factors such as nutrient availability might not be expected to change in unison. In this study, we produce a new long-term record of ε_p over the Oligocene to Miocene time interval at two new, widely separated locations: IODP Site1406 in the subtropical North Atlantic off the Newfoundland coast, and ODP 1168 in the Southern Ocean off Tasmania. We also increase the resolution of determinations at the equatorial Atlantic ODP 925. The existing ε_p -based CO₂ estimations for the Oligocene are derived from ~ 1 million year resolution measurements from two sites (Site 925 and 516) on the South American margin of the equatorial and South Atlantic; in the early Miocene an additional North Atlantic record (Site 608) provides data (CenCO2PIP Consortium, 2023). We also increase the resolution of determinations at the equatorial Atlantic ODP 925.

Our new <1 m.y. resolution ε_p records from these two mid- latitude locations allow us to directly compare ε_p with estimates of SST derived from alkenones extracted from the same samples, since unlike very warm tropical locations, the U_{37}^{kr} index still retains sensitivity to temperature in the mid-latitudes during the Oligocene and early Miocene. Additionally, we compare ε_p with benthic δ^{18} O available from the same sediments, an indicator of high latitude temperature and Antarctic ice sheet extent and/or volume. Variations in benthic δ^{18} O are controlled by changes in both deep-water temperature and deep ocean δ^{18} O_{sw} which reflects ice volume. We further measure ε_p and benthic δ^{18} O at approximately 20-30 ky resolution over a series of eccentricity cycles in the early Oligocene at IODP 1406. These long term relationships are contrasted with higher resolution analysis during the middle Oligocene at IODP 1406. The dataset allows a robust evaluation of the relationship between ε_p and climate dynamics for this time interval. We further discuss the significance of the observed ε_p record with the implications for the phytoplankton sensitivity over multimillion year timescales over the Cenozoic.

1.2 An overview of alkenone $\varepsilon_p p CO_2$ proxy

80

85

105

110

115

The carbon isotopic fractionation in phytoplankton during photosynthesis is affected not only by the aqueous carbon dioxide ($CO_{2[aq]}$) but also by physiological factors related to the cellular uptake of carbon. Physiological factors These were initially modelled from the assumption of diffusive carbon acquisition in phytoplankton cells (Rau et al., 1996), where higher ε_p could be induced by higher $CO_{2(aq)}$, lower instantaneous growth rates, or a higher cellular surface area to volume ratio. Both cellular permeability and the carbon isotopic fractionation by the Rubisco enzyme have been assumed to be constant, with Rubisco fractionation typically estimated between 25 and 29 ‰ for alkenone producers (Pagani et al., 2014). Traditional attempts to reconstruct pCO_2 from ε_p have simplified this original diffusive model by relating ε_p and CO_2 with a single factor b defined to include all physiological parameters affecting the fractionation, and ε_f representing the fractionation of the Rubisco enzyme (Jasper and Hayes, 1994).

(1)
$$\varepsilon_p = \varepsilon_f - \frac{b}{co2_{[aa]}}$$

The b-value has been estimated from modern photic zone and culture samples, for which $CO_{2(aq)}$ is independently known. For sedimentary alkenones, previous pCO₂ calculations have either, (1) assumed the modern b-value for that oceanographic setting remained constant in the past (e.g. Zhang et al., 2013), (2) applied modern relationships between b and phosphate and a simulated paleo surface ocean phosphate concentration at the site (Pagani et al., 2011), or (3) estimated the difference between the modern b value at the site and the paleo setting b value from productivity proxies or proxies for coccolithophore size (Bolton et al., 2016; Henderiks and Pagani, 2007). previous pCO₂ -calculates have either (1) assumed the modern b-value for that oceanographic setting remained constant in the past (e.g. Zhang et al., 2013), (2) applied modern relationships between b and phosphate and a simulated paleo-surface ocean phosphate concentration at the site (Pagani et al., 2011)-(3) estimated the difference between the modern b-value at the site and the paleo-setting b value from productivity proxies (Bolton et al., 2016) or (4) applied variation in the b-value at the site based on -proxies for coccolithophore size (Henderiks and Pagani, 2007). Despite the appeal of this approach, a recent re-evaluation of cultures and field observations suggest the b term is not well predicted by growth rate, light or cell size alone in a diffusive model but that .- Aadditional effects occur from carbon concentration mechanisms (CCM) on carbon uptake at lower CO2 concentrations, which cause a deviation in the CO2 dependence from the theoretical hyperbolic relationship (Hernández-Almeida et al., 2020; Stoll et al., 2019). A further challenge to the physical diffusive model is that the Rubisco fractionation in coccolithophores has been measured in-vitro as 11 % rather than 25% (Boller et al., 2011), suggesting that fractionations larger than 11% may reflect the operation of additional enzymatic fractionations (Wilkes et al., 2018). The lower Rubisco fractionation has implications for the has implies a lower sensitivity of ε_p to CO₂ (e.g. as explored in González-Lanchas et al. (2021)).

A meta-analysis of experimental culture data (Stoll et al., 2019) suggests that ε_p features a logarithmic dependence on CO₂, rather than the hyperbolic dependence implied by Rau et al. (1996). This approach analysis does not resolve the mechanisms for the observed relationship between ε_p and CO₂ slope of ε_p dependence on CO₂, but over the range of CO_{2(aq)} from 5 to 30 μ M, it provides an empirical relationship for interpreting the magnitude of CO_{2(aq)} change implied by a given ε_p change. The culture dataset illustrates more broadly how ε_p is the sum of its dependencies on ln(CO₂), ln(light), and growth rate μ_i and cell radius:

(2)
$$\epsilon_p = 2.66 \ln(CO_2) + 2.33 \ln(light) - 6.98 \mu_i - 1.28 \text{ radius} + 6.26$$

where CO_{2(aq)} is in μM, light is in μE, growth rate μ_i is day⁻¹ and radius is in microns (see Stoll et al. (2019) for confidence intervals on the regression).

From this empirical culture calibration, two challenges remain for the estimation of past CO_2 from ε_p measurements derived from sedimentary alkenones. First, its use would require an estimation of the cell radius, light during the season and depth of alkenone production, and the growth rate. While cell size can be estimated from coccolith length (Henderiks and Pagani, 2007), determining the absolute light and growth rate is rarely possible (Henderiks and Pagani, 2007). Since the equation is a linear sum of these influences, these non- CO_2 variables may be integrated into the intercept (e.g. as in González-Lanchas et al. (2021)), where the intercept (I) would decrease with higher growth rates and larger cell sizes and increase with higher light.

(3)
$$\varepsilon_p = 2.66 \ln(CO_2) + I$$

120

125

130

135

150

155

160

Yet, as with Eq. (21), there remains the challenge of determining which value should be used for the intercept for past conditions, and whether a constant or variable I is more appropriate for a given site since there are limited proxies for algal growth rate. Recent culture studies document a 0.5 % decrease in ε_p per 1°C warming (Torres Romero et al., 2024), and show that this magnitude is identical to the product of ε_p dependence on growth rate (Stoll et al., 2019) a magnitude which is indistinguishable from the prediction of growth rate effect on ε_p and the modeled temperature dependence of coccolithophore

growth rates (Krumhardt et al., 2017) <u>derived from diverse culture and field studies</u> (Behrenfeld et al., 2005; Fielding, 2013; Sherman et al., 2016). This suggests that growth rate, and I, may vary over time at a given location if temperature is variable. Therefore, records of SST from alkenone unsaturation or other proxies provide the opportunity to deconvolve the effects of temperature-driven growth rate variations on ε_p even when the absolute growth rate is not known.

In this study, given the potential for oceanographic conditions at the studied sites to differ significantly from those in the modern ocean at these locations, and the concomitant high uncertainties in estimating an appropriate *b* value for the traditional approach or *I* for Eq. (23), we do not calculate the past absolute CO₂ concentration from our ε_p measurements. Instead, we account for the potential influence of temperature-driven growth rate changes on our ε_p records using alkenone temperature estimates derived from the same samples. Similarly, we evaluate the potential impact of cell size variations on the ε_p changes.

Then, we employ the sensitivity of ε_p to CO₂ in Eq. (32) to estimate possible relative changes in CO₂ in the case where the other nutrient-stimulated growth rate or light influences on ε_p were constant during the studied interval at each site evaluating evidences for this assumption.

2 Sites and sediments

175

180

185

190

We have selected two widely separated paleo locations for this study, from the mid latitude North Atlantic encent and the high to mid latitudes of the Southern Ocean, from IODP 1406 (40°21.0′N, 51°39.0′W; 3,814 mbsl), ODP 1168 (43° 36.5′S, 144° 24.7′E, and 2463 mbsl), respectively (Fig. 1). A total of 43 and 34 sediment sampling spreading from 30 Ma to 17 Ma at each site were selected. Additionally, 61 samples (at approximately 15 ky sampling interval for bulk carbonate isotopes) were obtained from higher resolution sampling at IODP 1406 within the 30-29-30 Ma time window, of which 29 were processed for benthic foraminiferal isotopes and 22 yielded biomarkers sufficient for analysis. was performed within the 29-30 Ma time window. We also measured an additional six sample set from equatorial Site ODP 925 (4°12.25′N, 43°29.33′W, 3042 mbsl) in order to increase the million-year scale resolution of the previous longest Oligocene record in alkenone carbon fractionation (Zhang et al., 2013).

The age model for Sites 1406 and 1168 has been updated using new ⁸⁷Sr/⁸⁶Sr isotope stratigraphy (Stoll et al., 2024) and the age-modelling software Bacon (Blaauw and Christen, 2011). The new age model for IODP Site 1406 is comparable to previously published chronologies (e.g. as in Guitián et al. (2019) and Van Peer et al. (2017)) but clarifies the duration of the upper Miocene hiatus between 33.3 m and 34.7 m core depths (CCSF-A) as extending from 18.5 to 21 Ma. The ODP Site 1168 age model of ODP Site 1168—was revised with the Sr isotope stratigraphy in the interval from 562 to 278 mbsf. The Site 1168 chronology is significantly shifted for most of the Oligocene to early Miocene compared with previous biostratigraphically-based age models and shipboard magnetostratigraphy (Pfuhl and McCave, 2003). Strontium isotope stratigraphy identifies a condensed interval from 22.5 to 21.6 Ma, but suggests sustained sedimentation thereafter through 16 Ma. The age model is most uncertain between 27 and 25 Ma where the Sr isotopic curve has a low rate of change. For the two ODP 1168 samples deeper than the Sr isotope measurements (562 mbsf), and those from Site ODP 925 we use previous age constraints as published previously by Guitián et al. (2020).

The paleolatitude reconstruction for the Oligocene to early Miocene barely changes the position of Atlantic sites, in contrast, ODP 1168 moved from 55°S to 48°S between 30 and 15 Ma (Torsvik et al., 2012; van Hinsbergen et al., 2015). Paleoecological reconstructions from dinoflagellates confirm that the waters above Site 1168 were continually influenced by the Leeuwin Current and located well equatorward of the Subtropical Front (Hou et al., 2023b) Paleodepth estimates for coastal site ODP 1168 suggest a gradual deepening from the Eocene onwards (Exon et al., 2001).

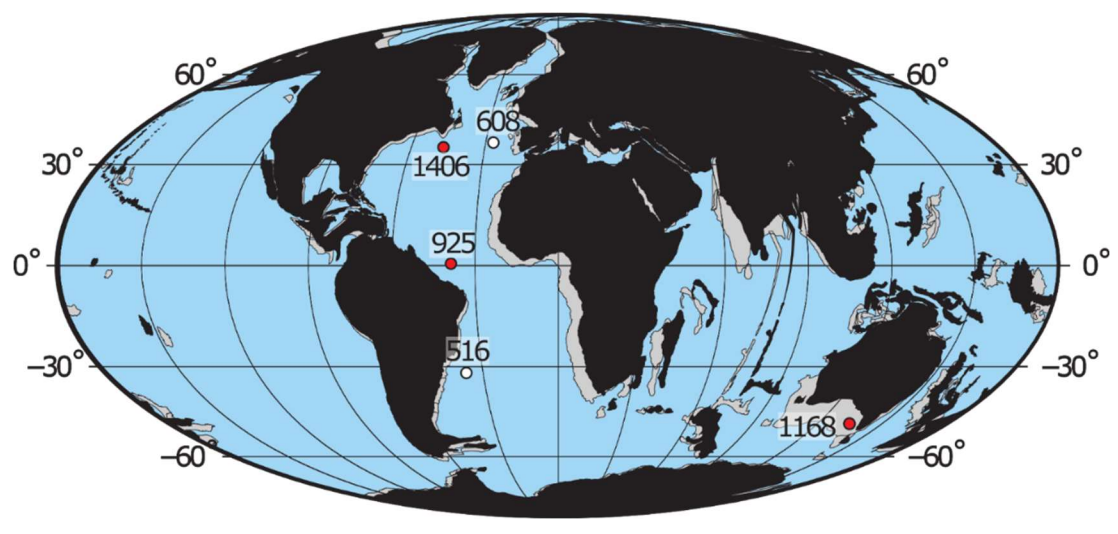


Figure 1. Location of the study sites. Reconstructed map of continental distribution over the 30 Ma (grey) – 17 Ma (black) time interval. Modified after the plate tectonic reconstruction service from the Ocean Drilling Stratigraphic Network (https://www.odsn.de/) using the data from Hay et al. (1999) ODSN.

3 Methods

200

205

225

3.1 Alkenone purification, quantification and δ^{13} C analysis

Biomarkers from sediments of IODP 1406 and ODP 1168 were extracted from 30g of freeze-dried sediment using an Accelerated Solvent Extractor 350 with CH₂Cl₂/MeOH (9:1 v/v) solvent for four static cycles at 100°C and further silica gel column chromatography protocols for purification of the ketone fraction containing the alkenones (see Guitián et al. (2019) for details).

Alkenone ratios were obtained with a Thermo Scientific Trace 1310 Gas Chromatograph (GC)-FID. Originally, for IODP 1406 and 1168 samples the GC-FID was equipped with a non-polar (60 m × 0.25 mm × 0.25 μm) capillary column (ZB-1ms, ZebronTM) at ETH Zurich and at Lamont-Doherty Earth Observatory from Columbia University (Guitián et al., 2019; Guitián and Stoll, 2021). However, ODP Site 1168 samples older than 22.4 Ma featured more complex chromatograms and a high diversity of compounds. To reduce the effects of coelution, samples were additionally analyzed on a 105m column RTX-200ms at ETH Zurich, which improved separation of long chain ketones (Rama-Corredor et al., 2018). The following temperature program was used: 1 min at 50°C, temperature gradient of 40°C/min to 200°C and 5°C/min to 300°C, hold for 45min, and increased to 320°C at 10°C/min and hold for 8min. Carrier gas was Helium at a flow rate of 1.5ml/min. In-house standards and replicates injected at every sequence ensured instrument precision. A subset of IODP Site 1406 and samples younger than 22.4 Ma from Site 1168 were re-measured with the RTX-200 to ensure replicability (Table S1). Method used for each organic analysis is described in the supplementary material dataset.

Sea surface temperature was calculated from $U_{37}^{k\prime}$ ratio using the Bayspline calibration (Tierney and Tingley, 2018) for all samples in IODP 1406 and for the young set (< 23.1 Ma) of samples in ODP 1168. Because for those, we find $U_{37}^{k\prime}$ ratios within the analytical uncertainty using both columns, we report the original ZB-1 results for all Site 1406 samples and Site 1168 samples younger than 22.4 Ma / 408.22 m depth. The RTX-200 column provided substantially improved resolution of C38 peaks, allowing quantification of C_{38:2} and C_{38:3} ME peaks₂₅ but fFor samples between the ages of 23.1 and 29.1 Ma in ODP 1168 it the RTX-200 column still did not perform sufficiently resolve coelutions on the C_{37:3} peaks well enough for all the C37 peaks. Therefore, for this set interval we provide temperatures estimated from the $U_{38ME}^{k\prime}$ ratio applying the Novak et al. (2022) core top calibration (Table S1). For the ODP 925 equatorial site samples, the C_{37:3} methyl ketone is under the detection limit,

therefore we further purified and analyzed the extracted organics as in Guitián et al. (2019) to get the temperatures from the TEX86 ratio using the BAYSPAR calibration by Tierney and Tingley (2015).

Compound-specific δ^{13} C measurements were performed on a Thermo Scientific Trace 1310 Gas Chromatograph coupled to a Thermo Scientific GC Isolink II, a Conflo IV, and a Delta V Plus Mass Spectrometer at ETH Zurich. Oxygen was flushed through the combustion reactor for one hour at the beginning of each sequence and seed oxidized for one minute before each injection. Alkenones from ODP Site 1168 and IODP 1406 were analyzed on a GC equipped with a non-polar capillary column $(60 \text{ m} \times 0.25 \text{ mm} \times 0.25 \text{ µm})$ (ZB-1ms, ZebronTM) and 5-m guard column. Helium was used as carrier gas flow with 2-ml/min. GC oven was set at to 90°C_{xz} ramped to 250 at 25°C/min, to 313°C at 1°C/min and finally to 320°C at 10°C /min. The GC oven was then maintained isothermally for 20 min. A subset of IODP 1406 samples were measured additionally at the Lamont-Doherty Earth Observatory on equivalent instrumentation but with some modifications for improved sensitivity (Baczynski et al., 2018) and following similar GC procedures, with similar results.

From ODP Site 1168, a subset of samples older than 24.5 Ma featuring more complex chromatograms were rerun on a GC-irMS equipped with a RTX-200 ms column. GC oven was set at 50°C ramped to 275°C at 40°C/min, to 295°C at 0.5°C, hold for 22 min, and finally ramped to 320°C at 10°C/min and hold for 5 min. Flow rate was 1.5ml/min. Comparison of a subset of samples from Site 1406 and ODP 1168 younger than 22.4 Mma showed that δ¹³C C37:2 were similar on both ZB-1 and RTX-200 columns. We consequently report here δ¹³C C37:2 from the ZB-1 runs, with the exception of the samples from Site 1168 older than 22.4 Ma. All values are reported here in parts per mil (‰) relative to VPDB (Vienna Pee Dee Belemnite). Sample replicates, in-house alkenone standard (provided by G. O'Neil, Western Washington University, and C. M. Reddy, Woods Hole Oceanographic Institution), and known isotopic mixtures A5 and B4 (supplied by A. Schimmelmann, Univ. of Indiana) were simultaneously measured to determine the analytical accuracy of the measurement and an uncertainty of 0.5 ‰.

3.2 Estimation of aqueous carbon dioxide δ^{13} C

235

255

260

265

250 Isotopic composition of CO_{2[aq]} is estimated from the temperature dependent fractionation between DIC and aqueous CO₂ during alkenone production of Rau et al. (1996) based on Mook et al. (1974) and Freeman and Hayes (1992):

(4)
$$\delta^{13}C_{[CO2]aq} = \delta^{13}C_{DIC} + 23.644 - \left(\frac{9701.5}{T}\right)$$

We calculate the δ^{13} C DIC from the δ^{13} C measured on the bulk carbonate, which is dominated by calcareous nannofossils, for which previous studies show *Reticulofenestra* to be the most abundant genera (Guitián et al., 2020). Because there is no divergence of vital effects between small and large coccoliths in the late Oligocene to early Miocene (Bolton and Stoll, 2013), we propose that the offset between coccolith δ^{13} C and DIC is likely to remain constant. We subtract 0.5 % from the δ^{13} C bulk to calculate δ^{13} C DIC, based on average alkenone-producing coccoliths cultured at DIC <4 mM compiled in Stoll et al. (2019). Support for estimating photosynthetic fractionation from coccolith δ^{13} C is provided by recent culture studies of *G. oceanica* (Torres Romero et al., 2024). In previous studies, the δ^{13} C DIC has also been estimated from the δ^{13} C of calcium carbonate of benthic foraminifera with the assumption of a constant and known offset between the δ^{13} C DIC of the deep and surface ocean. Although the foraminifera content in Site 1406 and 925 is very low, features sufficient well preserved benthic foraminifera, mainly epifaunal *Cibicidoides* spp. larger than 200 µm. At ODP Site 1168 benthic foraminifera were scarce for picking for isotopes in many intervals and the progressive evolution of water depth at the site may change the δ^{13} C offset between the benthic environment and the surface ocean over time (Exon et al., 2001). For an additional sensitivity test to evaluate the significance of the method of DIC estimation and facilitate comparison to other published ϵ_p records calculated from benthic δ^{13} C, we also estimate surface ocean DIC by adding a constant offset of +2 % to the δ^{13} C benthic measurements, following previous Miocene and Oligocene studies (Guitián et al., 2019; Pagani et al., 2011; Zhang et al., 2013).

The δ^{13} C DIC may be estimated from the δ^{13} C of calcium carbonate of benthic foraminifera with the assumption of a constant and known offset between the 813C DIC of the deep and surface ocean, or from bulk sediment calcium carbonate that is mostly derived from coccolithophores and planktonic foraminifera. Although the foraminifera content in Site 1406 and 925 is very low, Site 1406 and 925 features sufficient well preserved benthic foraminifera, mainly epifaunal Cibicidoides spp. larger than 200 μm, δ¹³C of surface ocean DIC can be calculated here applying a constant offset of 2 ‰ of measurements from the same samples following previous Miocene and Oligocene studies (Guitián et al., 2019; Pagani et al., 2011; Zhang et al., 2013). However, at ODP Site 1168 benthic foraminifera were scarce for picking for isotopes in many intervals and the progressive evolution of water depth at the site may change the δ^{13} C offset between the benthic environment and the surface ocean over time(Exon et al., 2001). Consequently, to follow the same approach for all studied records we calculate the δ^{13} C DIC from the δ¹³C measured on the of the bulk carbonate, which is dominated by calcareous nannofossils, for which previous studies show Reticulofenestra to be the most abundant genera coccoliths (Guitián et al., 2020). Because there is no divergence of vital effects between small and large coccoliths in the late Oligocene to early Miocene (Bolton and Stoll, 2013), we propose that the offset between coccolith δ¹³C and DIC is likely to remain constant. We subtract 0.5 % from the δ¹³C_{bulk} to calculate δ¹³C_{DIC}, based on average alkenone producing coccoliths cultured at DIC <4 mM compiled in Stoll et al. (2019). Support for estimating photosynthetic fractionation from coccolith δ^{13} C is provided by recent culture studies of G. oceanica (Torres Romero et al., 2024).

Stable isotopes of carbonates were measured Bulk carbonate and benthic foraminifera were measured using analytical techniques as described in in Guitián et al. (2019) with the guidelines from Breitenbach and Bernasconi (2011) for small carbonate samples on a GAS BENCH II Delta V Plus irMS from Thermo Scientific with international (NBS-19 & 18) and inhouse carbonate as standards achieving a precision of 0.07 ‰.

3.3 Calculation of $\varepsilon_{p\,37.2}$

270

275

280

285

300

305

Carbon isotopic fractionation (ε_p), describes the fractionation occurring during photosynthesis when carbon is fixed into algal cellular biomass ($\delta^{13}C_{org}$) from the ambient aqueous CO₂ ($\delta^{13}C_{CO2aq}$) (Freeman and Hayes, 1992):

(5)
$$\varepsilon_p = \left(\frac{\left(\delta^{13}C_{[CO2]aq} + 1000\right)}{\left(\delta^{13}C_{org} + 1000\right)} - 1\right) * 1000$$

Organic δ^{13} C is obtained from the δ^{13} C analysis of haptophyte specific alkenone di-unsaturated $C_{37,2}$. Culture experiments showed that the lipid organic matter is depleted in 13 C relative to the whole cell isotopic composition by 4.2 ‰, a correction that needs to be applied (Popp et al., 1998; Wilkes et al., 2018):

(6)
$$\delta^{13}C_{\text{org}} = [(\delta^{13}C_{37:2} + 1000) * ((4.2/1000) + 1) - 1000]$$

Uncertainties were propagated by a full Monte Carlo (n = 10000) simulation following Tanner et al. (2020).

To compare our new records with previous data spanning the same time interval, we discuss published ε_p datasets recently compiled by the paleo CO₂ community (CenCO2PIP Consortium, 2023), from DSDP 516 in the South Atlantic (Pagani et al., 2000; Pagani et al., 2011; Pagani et al., 2005), DSDP 608 in the North Atlantic (Super et al., 2018), and the equatorial site from ODP 925 (Zhang et al., 2013). For these, we ensure that ε_p for the published records is calculated from biomarker-based paleothermometers. The most recent publications from DSDP 608 and 925 used GDGT-derived estimations from TEX-86. To better compare our results with DSDP 516, where originally temperatures were derived from δ^{18} O of planktic foraminifera for the Miocene section and GDGTS for part of the Oligocene, we have updated the ε_p calculations using a running averaging of the recent higher resolution GDGT temperature reconstructions from Auderset et al. (2022) at the same site.

For our data of paired ε_p and alkenone SST, we calculate the shift in ε_p which is expected from temperature-stimulated growth rates. We adjusted each samples ε_p absolute value by uUsing the relationship of -0.48 % (95% CI = -0.37 to -0.95%) per 1°C SST _(Torres Romero et al., 2024), we adjusted each samples ε_p absolute value by using the _difference between the SST estimated for that sample and relative to the record average SST during the studied interval at that site (Torres Romero et al., 2024). We complete a similar exercise for cell radius, calculating the deviation in ε_p only relative to the median cell size, for each point using the culture dependence of ε_p on cell radius shown in equation (2+) (Stoll et al., 2019). Biogenic silica (bioSi) was determined on 20 samples from ODP 1168 following methods described previously in Guitián et al. (2020).

4 Results and Discussion

310

315

320

325

4.1 Trends in ε_p in the Oligocene to early Miocene

4.1.1 New ε_p records from sites 1406 and 1168

In both long-term records from Site 1406 and Site 1168, δ^{13} C of $C_{37.2}$ alkenones range from very low values near -30 % in the early Oligocene (30-28-30 Ma) increasing to -24 % by 20-18-20 Ma (Fig. 2). The new calculated ε_p decrease from the Oligocene to the early Miocene, defined most precisely at the highest resolution North Atlantic Site 1406, features abrupt 3 % declines from 27 6.5 to 254.45 Ma and 24 to 22.8 Ma. At ODP 1168 the lack of ε_p ep-measurements prior to 25 Ma hinders identification of a clear transition. Newly obtained ODP 925 ε_p determinations within the interval 25 Ma to 19 Ma are in agreement with previous determinations at this site (Zhang et al., 2013) resolving showing also the broad interval of ε_p decreasestep from s at 27.6 ma and to 24.5 21-Ma. The trends in ε_p calculated from benthic δ^{13} C are similar to those calculated from the coccolith-dominated bulk δ^{13} C. In the high resolution section from 29.6 to 28.8 28.8 to 29.6 Ma in Site 1406 there is no long-term trend, but orbital scale ε_p variations exceed 1.5 % in amplitude (Fig. 3, Fig. S1). Over several ~100 ky orbital cycles, Several ~100 ky orbital scale variations of 0.75 % benthic δ^{18} O and bulk δ^{18} O in other sites during this time period (Liebrand et al., 2017).

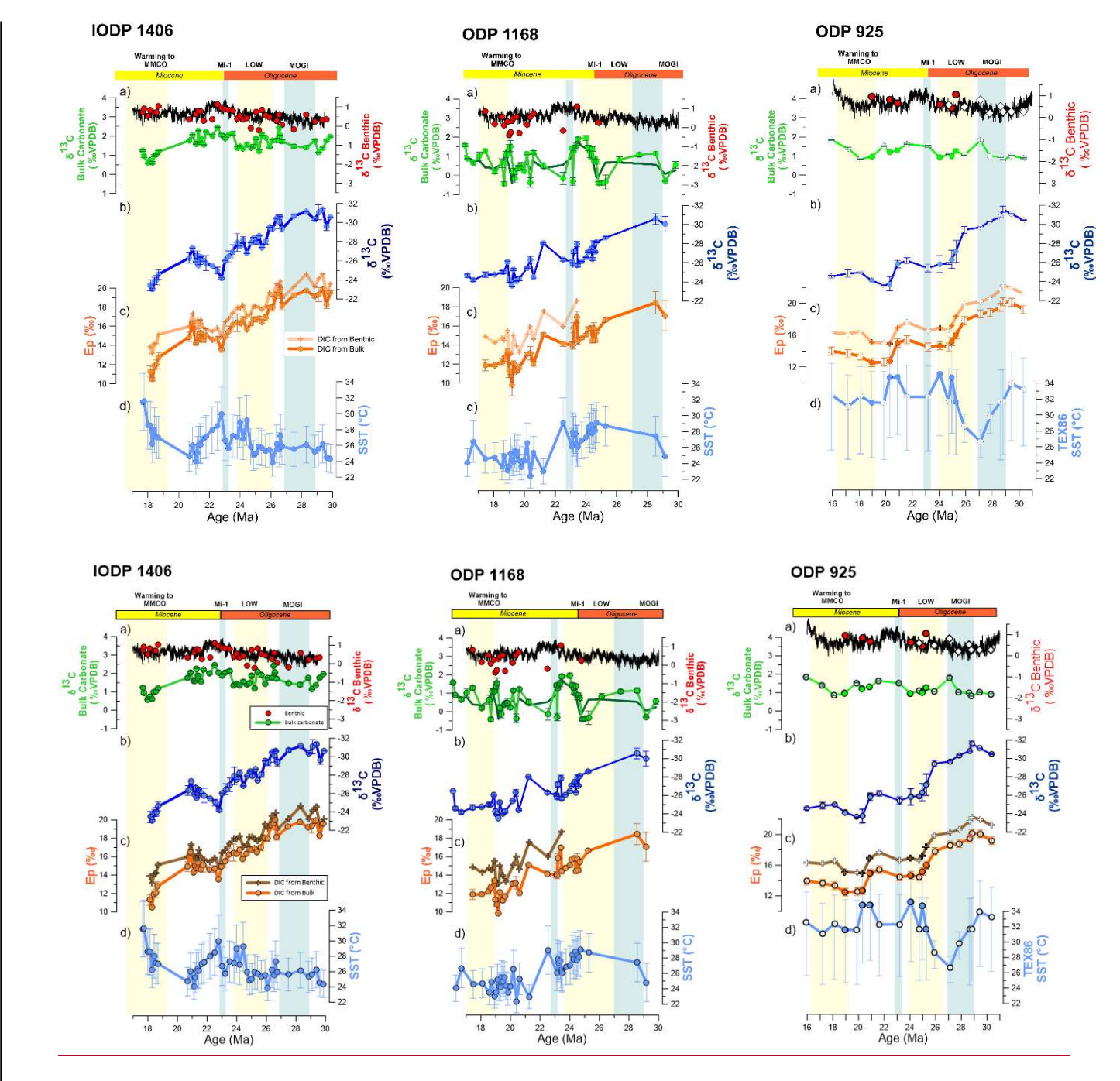


Figure 2: Analytical results of this study. a) Carbonate stable isotopes for benthic foraminifera (red symbols), data from this work for each site; black line shows results from Westerhold et al., (2020) and bulk sediment carbonate (green color). b) Alkenone C_{37.2} δ¹³C. c) Calculated alkenone carbon fractionation, solid line DIC δ¹³C is derived from bulk carbonate, transparent line from picked benthic foraminifera at the same samples. d) Temperature estimates. IODP 1406, including SST and benthic δ¹⁸O dataset from Guitian et al., (2019); ODP 1168, dark green δ¹³C bulk carbonate shows the 4-point moving average used to calculate εp at the site; ODP 925, filled circles are new measurements for this study, white symbols are published data (Zhang et al., 2013), being ε_p recalculated following method described in text. Note SST is derived from GDGT at this site. Alkenone SST-derived show errors bars: 1406–1σ error bars and GDGTs, 1168 U^{kt}/₃₃₇–1σ, 1168 U^{kt}/_{338ME}-2σ, 925-TEX86-refer to 2σ.

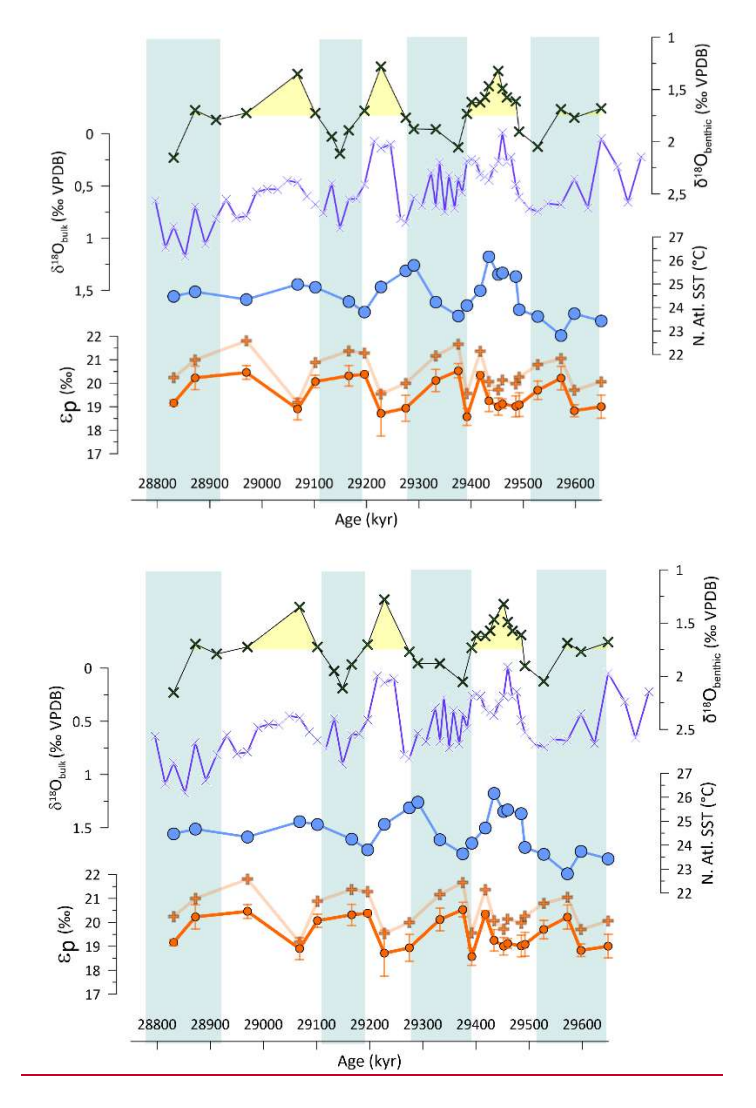


Figure 3. High resolution sampling from IODP 1406, showing δ^{18} O of bulk carbonate and benthic foraminifera, alkenone SST estimates, and ϵ_p calculated from bulk carbonate (circles) and benthic foraminifera assuming a constant offset (crosses).

4.1.2 Comparison of 1168 and 1406 ε_p records with published Atlantic records

345

350

355

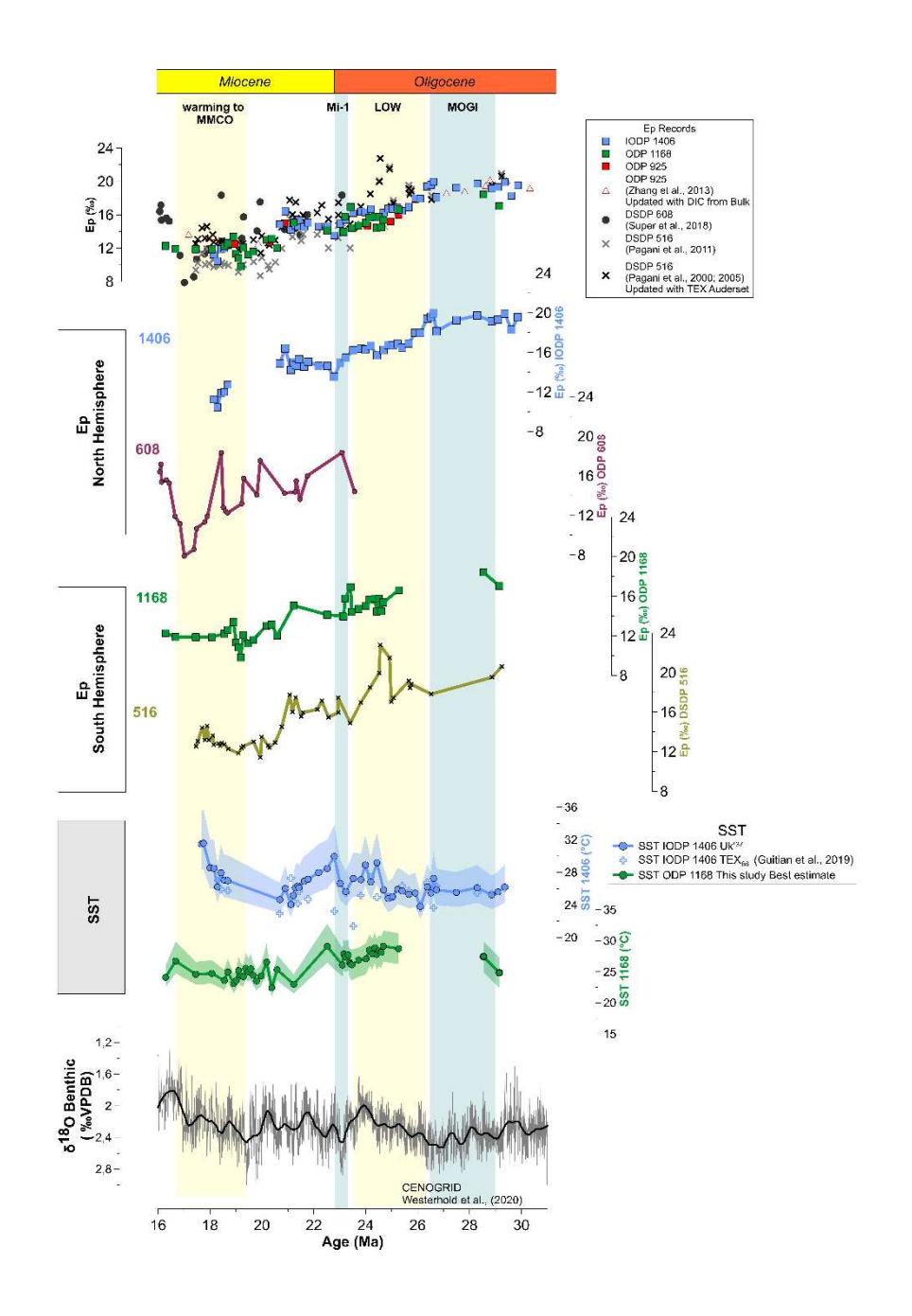
The overall decline in ε_p through the time interval of our records, is broadly comparable to the trend in published ε_p datasets recently compiled by the paleo CO₂ community (CenCO2PIP Consortium, 2023), which exhibits a long term decrease in the late Oligocene through the transition to the Miocene and to overall low and stable values in the early Miocene and overall low and stable early Miocene (Fig. 4). However, several factors complicate a detailed comparison of our new and the previously published records.

Correlation of Rrapid ε_p shifts comparison might be hindered by uncertainties in chronology among the different sites chronology uncertainties. Although all records are presented here on the GTS 2012 (Gradstein et al., 2012), ODP 1168 and IODP 1406 age models rely on Sr isotope stratigraphy (Stoll et al., 2024), whereas ODP 925, DSDP 516 and ODP 608 are based exclusively on biostratigraphic and magnetostratigraphic reversals datums (Consortium, 2023; Curry et al., 1995; Guitián et al., 2020). As previous studies document for seen in sites 1168 and 1406, Sr isotopic stratigraphy can adjust age determinations by 0.5 to 1 Myr- or even up to 2 Myr- in a at few cases (Stoll et al., 2024).

Additionally, differences in the absolute value of ε_p among records may also reflect contrasting approaches to the reconstruction of DIC δ^{13} C in the different studies. At DSDP 608, the DIC δ^{13} C was reconstructed from surface-dwelling foraminifera *G. quadrilobatus* (Pagani et al., 1999), while at DSDP 516 the Miocene section was estimated from planktic foraminifera and most of the Oligocene samples DIC δ^{13} C was determined from fine fraction (Pagani et al., 2000; Pagani et

al., 2005). Published ODP 925 ε_p has been recalculated here with DIC δ^{13} C derived from bulk carbonates of nearby samples, to resolve the previous divergent estimates from planktic and benthic foraminifera (Zhang et al., 2013).

The longest record from DSDP Site 516 exhibits a general ε_p decline from the Oligocene to early Miocene. -However, due to lower resolution at this site, we cannot evaluate if there is an abrupt 3 ‰ decline from 276.5 to 24.5 Ma as seen in sites 1406 and 925. A steep ε_p decline between at 21 and 20 Ma in Site 516 may be within age uncertainty of the decrease observed between 20 and 19 Ma at ODP 1168 and ODP 925; additional Sr isotope stratigraphy at Site 516 in this time interval could help test the synchronicity. The late Oligocene at DSDP 516 features a a-transient 5‰ positive excursion peak increase in ε_p between 24.5 and 24.9 Ma, which is not reflected at 1406, or 1168 sites. With current information, we cannot assess if this difference reflects age model uncertainty, potentially unresolved coelutions -analytical uncertainty-from GC-IRMS chromatography, or aliasing. The early Miocene record at DSDP Site 608 shows a more variable ε_p with a much steeper decline through the early Miocene and higher amplitude variation compared to other sites. The characteristic minimum in ε_p from 18 to 17 Ma is potentially within the age model uncertainty of the 19 Ma minimum in ε_p at 19 Ma in 1168 and the 18.5 Ma minimum identified at Site 1406 at 18.5 Ma. Updated stratigraphy could contrast more robustly the timing of these events. If there is high amplitude short term variability in ε_p in the early Miocene as in the Oligocene time interval (Fig. 2), there is also the potential for low resolution sampling to undersample high frequency temporal variability and generate aliasing artefacts.



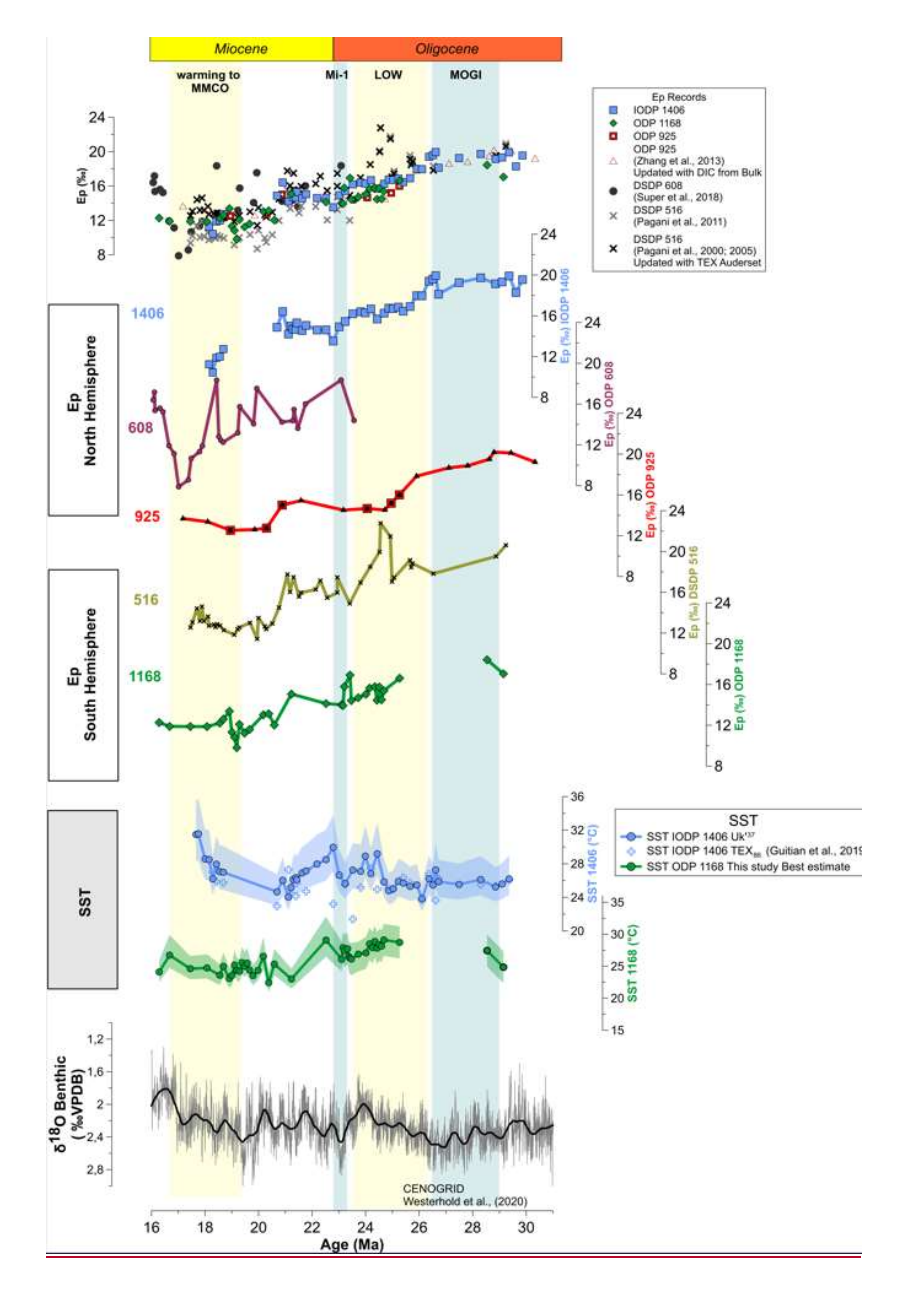


Figure 4: Oligocene to Miocene global long term ε_p trends. Comparison of the new obtained ε_p records with previously published alkenone measurements. All ε_p estimates have been recalculated following the methodology described in text with data source described on Table S2.

4.2 Potential for size and nutrient effects on CO₂-vs size and nutrient effects on ε_p

380

385

In addition to CO₂, ε_p may be influenced by changes in <u>cell surface area to volume ratiocell size</u> and cellular growth rate regulated by light and nutrients. There is no long-term trend in mean coccolith size in these records (Guitián et al., 2020) and estimating the impact of it on the ε_p records shows a negligible effect on long-term trends (Fig. 5). At discrete time intervals of IODP Site 1406, the <u>correction for the</u> size effect reduces most values older than 27 Ma and produces a steeper decrease on ε_p towards the Oligocene Miocene transition.

For the statistical model of Eq. ($\underline{24}$), it is complex to identify proxy records for any possible effect of nutrient-stimulation of growth rate or changes in the mean light conditions at the depth of growth. In modern spatial gradients in the ocean, these factors are often coupled, so that settings characterized by deep mixing and high nutrient supply rates to stimulate growth, are also characterized by lower mean light levels due to the deeper mixing, both factors lowering $\varepsilon_{p_{\underline{a}}}$ (Hernández-Almeida et al., 2020).

As one possible nutrient indicator, a higher concentration of biogenic silica (bioSi) in sediments may reflect a higher rate of bioSi delivery to the seafloor due to higher export production produced by siliceous organisms (mainly diatoms) in the ocean (Ragueneau et al., 2000). In the modern ocean, regions with abundant dissolved Si in the photic zone are regions also characterized by higher concentrations of macronutrients such as P and N. However, bioSi is an imperfect indicator of past surface nutrient content because coccolithophores have a minimal Si requirement, and Si remineralization in the ocean does not occur at the same rate as soft-tissue nutrients such as N and P. At IODP 1406, bioSi concentrations generally increase from the Oligocene to earliest Miocene, potentially indicating a gradual increase in the concentration of dissolved Si in surface waters at the site (Fig. 5). If the increase in dissolved silica observed at the North Atlantic is correlated to an increase in dissolved P or N, it could contribute to increase in growth rate, and therefore likely increase in biomass and chlorophyll, which would reduce light in the water column, both factors potentially contributing to both being part of the observed long term decrease of ε_p . However, the actual correlation between bioSi and ε_p is not that strong (Fig. S2), suggesting that while increased nutrient concentrations could contribute to the long-term evolution of ε_p , the specific steps of ε_p decline are less likely to be driven by increased nutrients and growth rate.

The drivers for increasing bioSi burial rates at Site 1406 are not clear, although they could reflect a global increase in nutrient delivery or local effects. Important changes in the rate of continental weathering within the Oligocene- early Miocene are often interpreted from the evolution of radiogenic isotopes of Sr, Li and Os (Misra and Froelich, 2012) including the steep rise in 87Sr/86Sr, although the precise origin of the late Eocene and Miocene increase in 87Sr/86Sr remains under discussion (Rugenstein et al., 2019). On a global scale, the nutrient delivery may be conditioned by the riverine supply of P from continental erosion and weathering of P containing minerals. Yet, oon the time scales examined in our records, much longer than the residence time of P, the net effect on nutrient concentrations depends on the balance of the supply and the nutrient removal in sediments.

While a significant increase in erosion and weathering and nutrient inventory is one mechanism to contribute to the long term decline in ε_p via enhanced algal growth rates, an increase in erosion and weathering can itself contribute to a CO₂ drawdown by CO₂ consumption through silicate weathering and enhanced burial of organic carbon in delta regions (Raymo and Ruddiman, 1992). If the biogenic Si increase at 1406 were representative of a global trend, an increase in nutrient supply may have contributed to ε_p decline through both CO₂ decline and increased nutrient stimulation of phytoplankton growth. A global decline in ε_p solely from increased weathering and nutrient concentrations without a CO₂ decline would require that in the Oligocene, the nutrient release from silicate weathering was less coupled to carbon burial than in the late Neogene. If the periodically glaciated margin of Antarctica is a major locus for increased erosion and weathering in the Oligocene (Reilly et al., 2002), release of nutrients and radiogenic isotopes may have occurred in the continental margins, but with much less organic carbon burial than the modern Himalaya system due to limited terrestrial biomass on Antarctica and temperature and sea-ice limited oceanic biomass production in the marine regions.

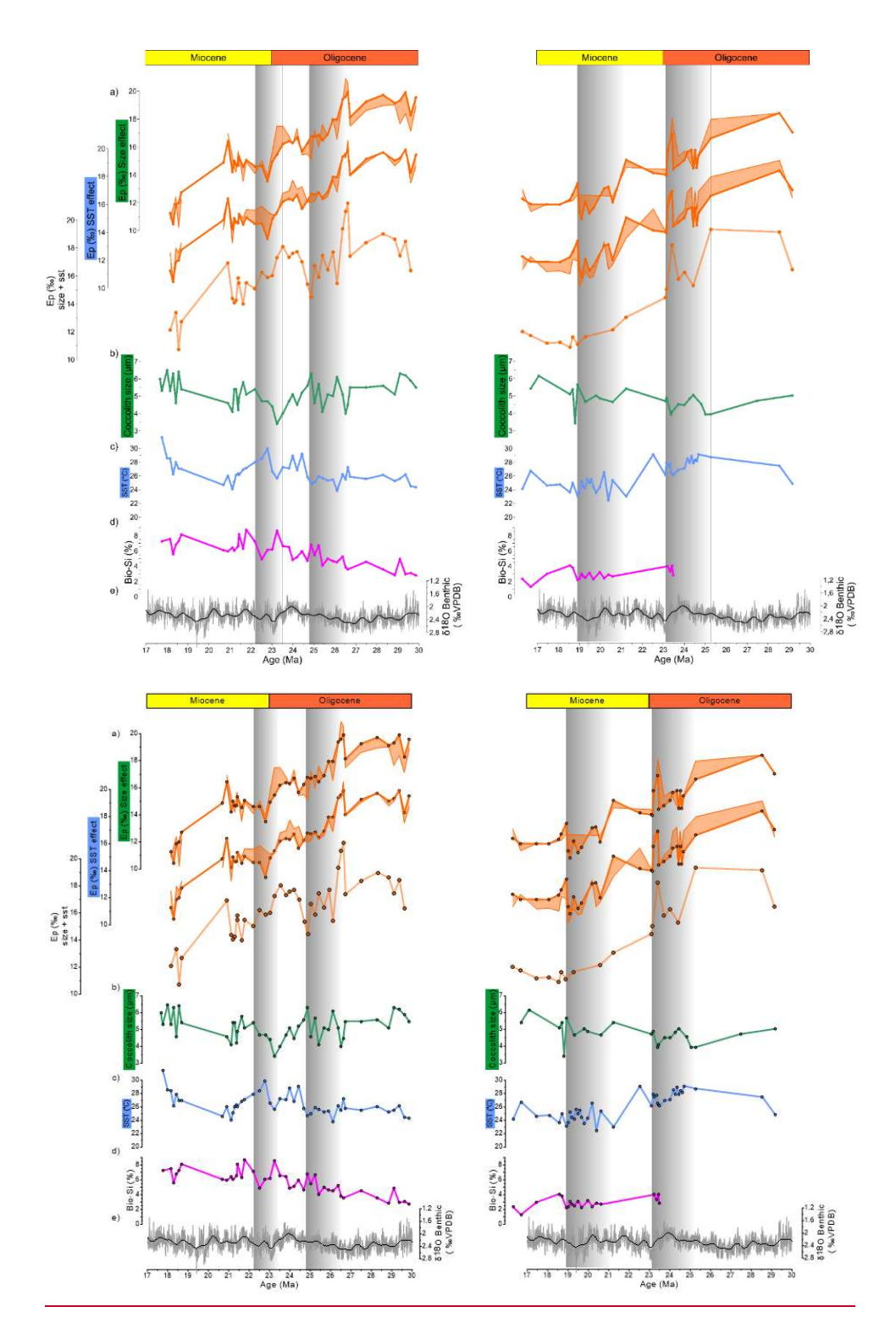


Figure 5: Timeseries of ϵ_p at IODP 1406 and ODP 1168 including a) the measured $\underline{\epsilon_p}$ ep-record (solid line) and the estimated ϵ_p resulted once size and temperature effect is applied following Torres et al., (2024), and Stoll et al., (2019) (transparent shadows). b) Coccolith size record from Guitian et al., (2020); c) SST estimates d) Biogenic silica measurements (Guitian et al., (2020) and this study); e) reference CENOGRID benthic δ^{18} O curve (Westerhold et al., 2020)

425

430

On the other hand, the long term trend of increased bioSi is not observed in the Southern ocean Site 1168 (Fig. 5). The available Miocene bioSi at ODP 1168 is stable with no change across the steep ε_p -drop from the latest Oligocene to early Miocene. The increasing distance of Site 1168 from the coastline with basin subsidence may have decreased the availability of Si from the early Oligocene through the early Miocene, imparting a local effect superimposed on any potential global trend. However, likely not only Si but also other nutrients would decrease with increasing distance from the coast. If the long term trend in ε_p at both 1406 and 1168 sites were conditioned by increased nutrient availability, faster growth rates, and lower light levels it would require bioSi accumulation rates at Site 1168 to be decoupled from the overall changes in nutrient availability, which

we consider less likely. Consequently, we propose that the similarity in trend and magnitude of the long term ε_p decline in both sites (and in tropical Site 925), is more consistent with a global forcing of ε_p, which may be most plausibly driven by a significant decrease in atmospheric CO₂ and CO₂aq.

4.3 Relationship between ϵ_p and SST and benthic $\delta^{18}O$

The new ε_p data from Site 1406 and Site 1168 provide the first records of ε_p from the early Oligocene to early Miocene with alkenone unsaturation indices as independent estimations of SST for the precise time intervals of ε_p determination. Since they are biomarkers derived from the same organism, alkenone-derived SST estimates correspond to the same season and growth depth as the alkenone ε_p determinations. There are two processes which may influence the relationship between temperature and ε_p . First, higher temperatures lead to higher phytoplankton carbon fixation rates, decreasing ε_p . Secondly, higher CO₂ would increase ε_p and through radiative forcing lead to warmer global average temperature and SSTs. The expected relationship between ε_p and SST from either process could be obscured by a superposition of temperature effects on growth rate and a climatic correlation of ε_p with mean air temperature.

4.3.1 Million year scale relationships

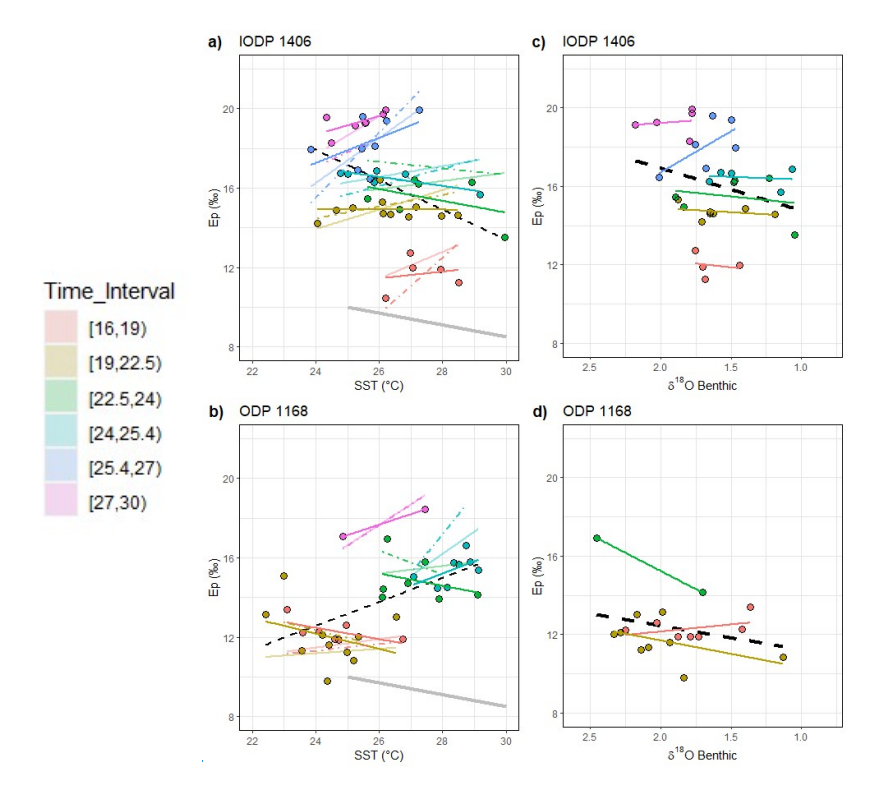
440

445

450

455

Across the overall time interval, Site 1406 ε_p is weakly inversely correlated with SST, whereas Site 1168 ε_p is weakly positively correlated with SST (Fig. 6; Fig. S3, Table S3). Our estimation of the growth rate effect due to warmer temperatures shows that it has a very limited impact on the long term ε_p trend, amplifying slightly the long-term excursion in ODP 1168 and imparting a minor increase in ε_p in the late Oligocene 25.5 to 24 Ma in IODP 1406 but otherwise not affecting the sign of the overall trend (Fig. 5, 6, Fig. S3). At our studied sites across the 30 to 17 Ma time interval, the long term average warming of 2-3°C is insufficient to account for the 7 ‰ decline in ε_p due to a temperature-driven growth rate effect. Unlike alkenone-based SST, the published TEX86 SST record at Site 1168 (Hou et al., 2023a) does not indicate a transition to lower temperatures from the Oligocene to early Miocene, suggesting different temperature trends in the season or depth niches of the different proxy carriers.



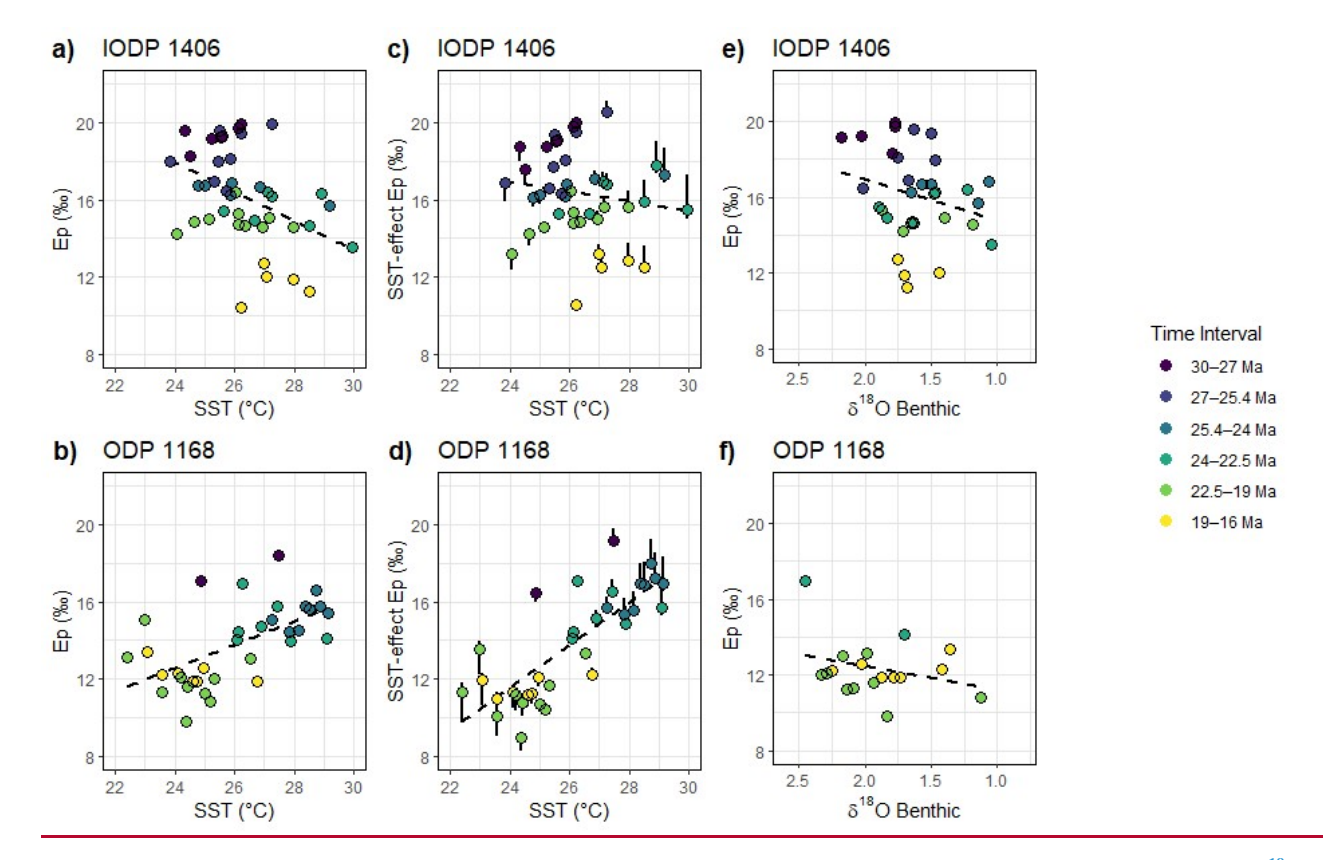


Figure 6. (a-b) For paired samples, Rrelationships between the measured between calculated ε_p and SST and benthic δ¹⁸O for the same samples from IODP 1406 and ODP 1168 between measured ε_p and SST_τ for Site 1406 and 1168. (ca-bd) Relationship between SST and ε_p, when the temperature-dependent growth rate effect on ε_p has been removed using the observed dependence of from culture experiments of without the cultures theoretical temperature effect of 0.5‰ (0.37 ‰ – 0.95‰ range indicated by error bars) decrease inchange ε_p per 1°C warming (Torres Romero et al., 2024), and SST (e-d)(e-f) For paired samples, measured ε_p and benthic δ¹⁸O-(e-f). Dashed dark line in the plot background shows the regression for of the overall dataset. Grey line in a) b) shows empirical temperature growth rate effect in temperature described in the text (Torres et al., 2024) as the ε_p-change with growth rate if CO₂ were constant. Colored lines shows the regression at specific time intervals for the measured ε_p (solid), ε_p with the temperature effect removed (transparent), and ε_p with both the temperature and size effect removed (dashed). See Fig. S3 and Table S3 for overall dataset statistical relationships.

Yet aside from the overall inverse correlation at IODP 1406, during certain time intervals the correlation is positive. Before 25.4 Ma, there is a general positive correlation between ε_p and alkenone SST (Fig. 6, Table S3); for the intervals $\underline{27}$ to $\underline{30}$ and $\underline{25.4}$ to $\underline{27}$ Ma in Site 1406 with a slope of 0.7 (n=6, n=10). This is also true for the $\underline{25.4}$ to $\underline{24}$ Ma interval in 1168 with 0.6 slope (n=6). This slope is significantly greater when the influence of size and temperature growth rate effects on ε_p are removed. In other time intervals, there is a negligible slope or negative slope with measured ε_p , for example -0.3 ($\underline{24}$ to $\underline{22.5}$ Ma in both sites, n=7, n=4) or during the drop after $\underline{19}$ Ma at IODP1406 appear to occur at times of warming temperature (slope=0.2, n=5) that slightly improves when the ε_p is adjusted to size and temperature.

470

475

480

Over the studied time interval, <u>SST and this ε_p relationship</u> similarly shows insignificant correlation for the previously published ε_p , records with updated age models and ε_p calculations (Fig. S4), although temperatures estimates are derived from GDGTs which might not reflect the same depth and/or season of coccolithophore growth. Negative covariance is observed at DSDP 608 from 19 to 16 ma, at DSDP 516 before 21 Ma and for the few samples from 27 to 24 Mma at ODP 925. Some of these intervals feature significant temperature changes of 4 to 5°C, and therefore the temperature-growth rate effect on ε_p may be significant, and the negative slopes observed in some intervals are consistent with this being the dominant effect (gray line in Fig. 6a and 6b). At 1406, during the older intervals of positive correlation of SST and ε_p , potentially the growth rate stimulation due to higher SST was balanced by a decrease of nutrient availability during warmer temperatures as suggested by the bioSi evolution (Fig. S2), whereas during younger time intervals, temperature exerted a dominant effect on growth rate.

Benthic δ¹⁸O was measured in multiple time intervals in Site 1406. Benthic δ¹⁸O has been proposed to reflect global surface temperature (Evans et al., 2024; Hansen et al., 2013) and as such may be less sensitive than SST to regional reorganizations of heat transport. Alternatively, benthic δ¹⁸O has been proposed to be highly sensitive to the areal extent of the Antarctic ice sheet due to its cooling effect on surface ocean temperatures in regions of deepwater formation (Bradshaw et al., 2021; Lisiecki and Raymo, 2005; Shackleton, 1987). If the global surface temperature change translated to changes in surface ocean temperatures at Site 1406 and Site 1168, we would expect the temperature-growth rate effect to generate a direct correlation between benthic δ¹⁸O and ε_p. If the radiative forcing effect on global temperature change were dominant, we would expect an inverse correlation between ε_p and benthic δ¹⁸O. As for SST, only the time intervals older than 25.4 Ma exhibit the inverse correlation expected from radiative forcing, whereas other intervals suggest neutral slope which may reflect the superposition of growth rate and CO₂-radiative effects on ε_p.

4.3.2 Relationships between ε_p , temperature and benthic $\delta^{18}O$ at orbital timescales

495

500

In the high resolution sampling between 29.0 and 29.6 Ma, despite a significant 1 % range in $\delta^{18}O$ benthic and $\delta^{18}O$ bulk, we likewise observe no inverse relationship between ϵ_p and $\delta^{18}O$ benthic, or between ϵ_p and $\delta^{18}O$ bulk (Fig. 7). We also observe no significant correlation between ϵ_p and alkenone SST. Because the magnitude of SST variation is small over this time interval, the impact of temperature-stimulated carbon fixation rates is not a significant impact on the relationship between ϵ_p and SST or $\delta^{18}O$ benthic any of these variables – a temperature-corrected ϵ_p record for the 29.6 to 29.6 Ma interval would still not exhibit an inverse relationship between ϵ_p and $\delta^{18}O$ benthic as observed in the late Pleistocene glacial cycles (Hernández-Almeida et al., 2023). If ϵ_p variations are dominantly responding to CO_2 , our results suggest that low CO_2 is not contributing to greater ice volume and/or colder ocean temperatures on 100 ky cycles and that the relationship between Antarctic ice growth and CO_2 may be more complex at this time.

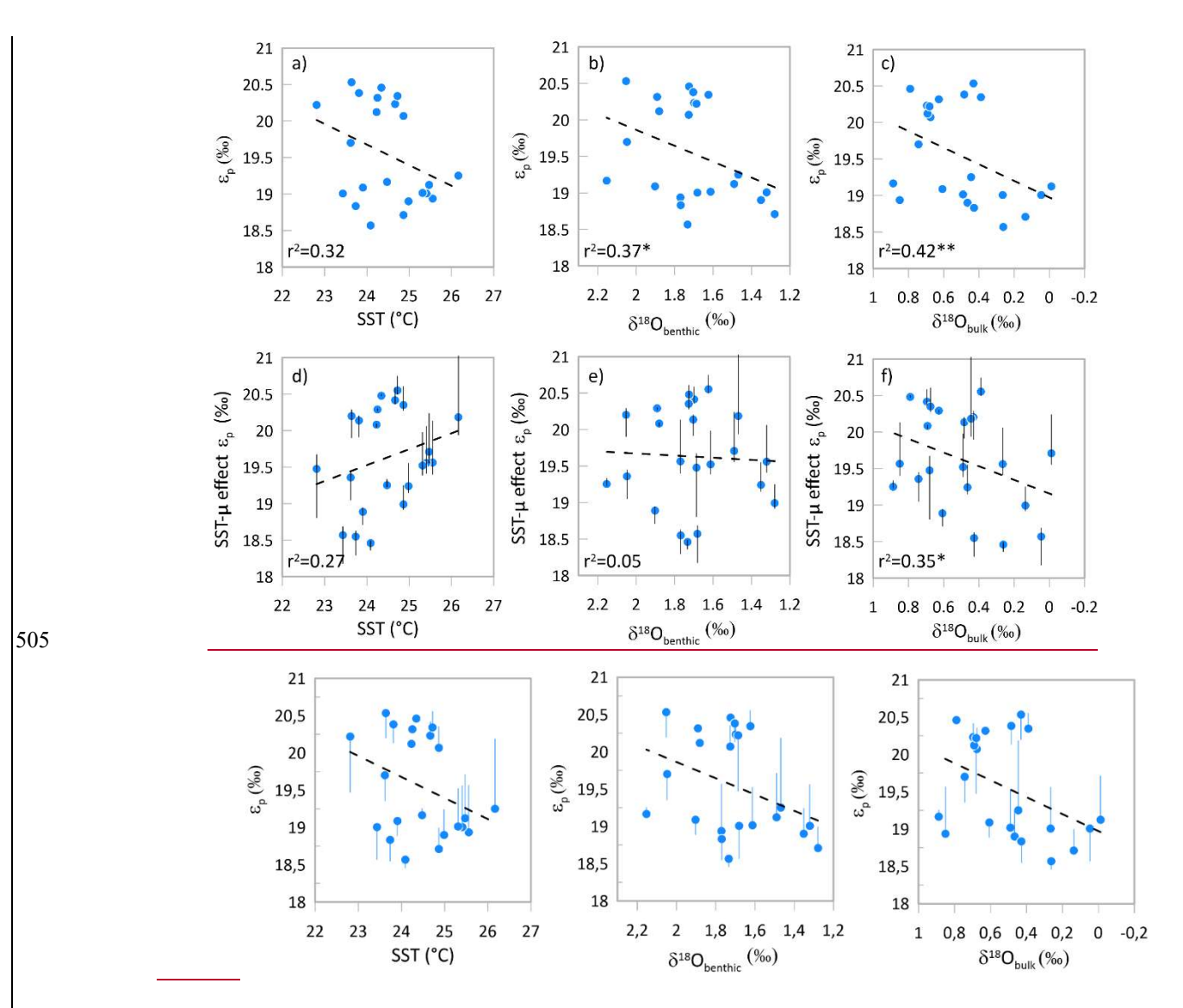


Figure 7. For the high resolution 29 to 29.6 Ma interval at Site 1406, Rrelationship between calculated ε_p and a) temperature (r²=0.34), b) δ¹⁸O from benthic foraminifera (r²2=0.42), and e) δ¹⁸O from bulk carbonates (r2²=0.37) for the high resolution interval samples from IODP 1406. Panels a) through c) illustrate the measured ε_p. In panels d), e) and f) ε_p is corrected for temperature-driven growth rate variation, for using the Vertical error bars shows the temperature effect on ε_p following findings from cultures of 0.5 ‰ per 1°C (Torres et al., 2024). Vertical error bars illustrate ε_p values when the slope of the correction ranges from 0.37 (light blue) to 0.95 ‰ (dark blue) per 1°C warming. Dashed line shows the linear regression for all plotted samples. *p value <0.1, **p value <0.05

4.4 A Climate and CO₂ paradox from the Oligocene to early Miocene

520

525

The long term trends between 30 and 16 Ma based on new ε_p data at two sites and recalculation of previous ε_p studies with uniform methods cannot be attributed to a temperature effect on growth rate and ε_p , nor to changes in the cell size of the alkenone producing community. Both effects are small in magnitude according to the sensitivities observed in cultures and do not alter the long-term trend (Fig. 5). Therefore, the long-term ε_p decline must have a significant global driver, with the most obvious being a decline in pCO_2 .

Although the calculation of absolute CO_2 concentrations from ε_p in the Oligocene and early Miocene remains challenging, the logarithmic dependence of ε_p on $CO_{2[aq]}$ observed in cultures allows us to estimate the relative changes in CO_2 if the sensitivity of ε_p to CO_2 in the Oligocene were similar to modern cultured species. If we incorporate a temperature correction on growth rate (Krumhardt et al., 2017) equivalent to the magnitude from cultures (Torres Romero et al., 2024) and apply the 50^{th} percentile estimate of the modern culture ε_p dependence on $ln [CO_{2[aq]}]$ of 2.66, it implies major changes in CO_2 concentrations, with potentially 4 halvings of CO_2 concentration from 29 to 16 Ma (Fig. 8). Modern General Circulation Models (GCM) estimate climate sensitivity at 3 to $5^{\circ}C$ per doubling or halving of CO_2 , which if representative for the Oligocene to early

Miocene, would imply 12 to 20°C of cooling of earth's mean surface temperature. Although ocean is 70% of the globe and temperature changes are 1.3- to 1.8-fold less than land temperature (Sutton et al., 2007), such a large temperature change of at least 10.4°C would be expected to be reflected in paleoceanographic proxies. Application of the lower confidence interval of modern culture ϵ_p dependence on $\log(CO_{2[aq]})$ of 3.5, would imply 3 halvings of CO_2 , with a correspondingly lower magnitude of change in temperature.

530

535

Similar to phytoplankton proxy records, the available low resolution leaf gas CO_2 records suggest a decline in CO_2 from the mid to latest Oligocene. However, in contrast to phytoplankton proxy records indicating for a significant long term decline in CO_2 from the early Oligocene through mid-Miocene, leaf gas CO_2 proxies suggest higher CO_2 in the early Miocene than the Oligocene due to a positive shift across the OMT. Boron isotope-based CO_2 records from 24 to 18 Ma show significant variability with no clear trend, although the higher density of data around the OMT suggests a CO_2 rise from 23 to 20 Ma which may be consistent with the trend observed in the ε_p record at Site 1406, which has the highest resolution for this time interval.

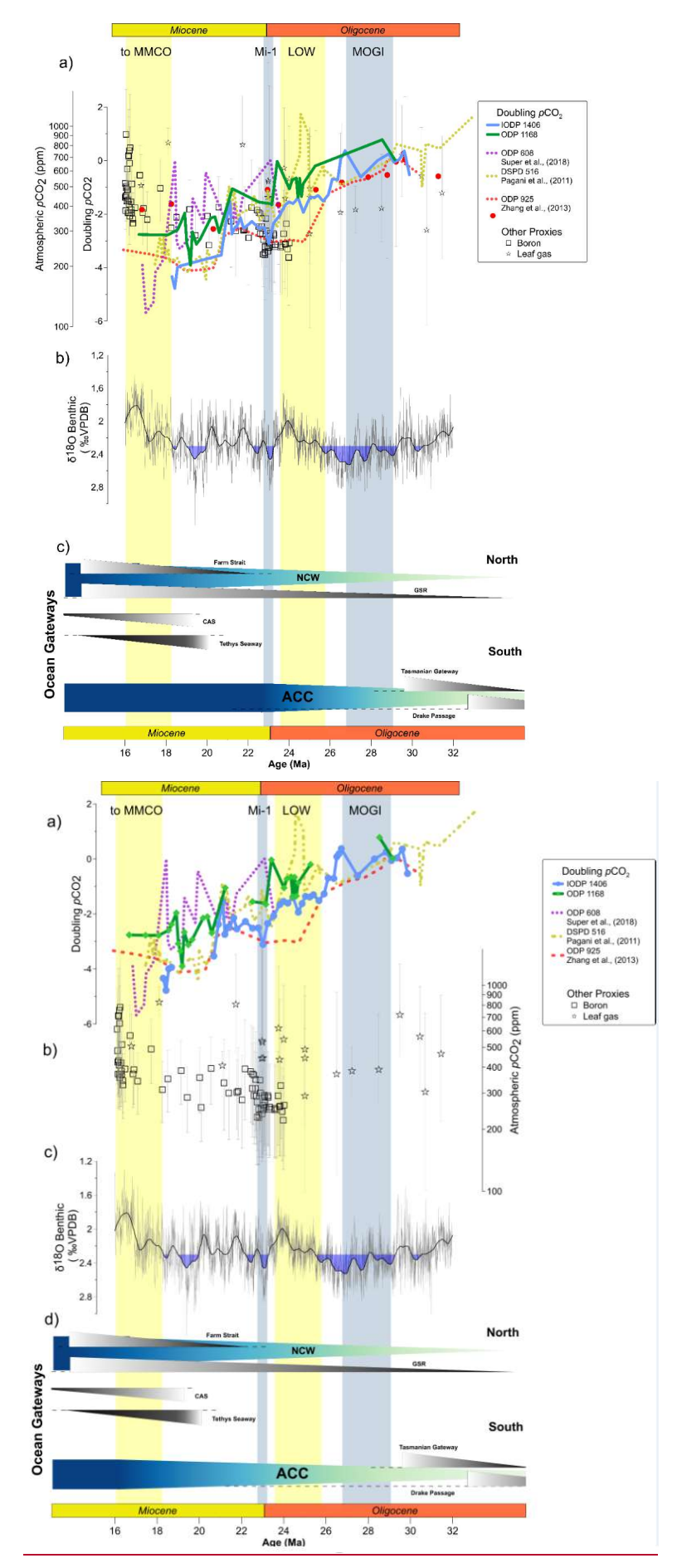


Figure 8: Implications of CO₂ as main climate driver. a) Shows pCO₂ doubling for the discussed sites b) pCO₂ estimates from boron and leaf gas compared to previous estimates compiled in CenCO2PIP Consortium, (2023) (Erdei et al., 2012; Greenop et al., 2019; Liang et al., 2022a; Liang et al., 2022b; Londoño et al., 2018; Moraweck et al., 2019; Reichgelt et al., 2020; Roth-Nebelsick et al., 2014; Sosdian et al., 2018; Steinthorsdottir et al., 2021; Sun et al., 2017; Tesfamichael et al., 2017; Zhang et al., 2013). Only long

545 term records from alkenone derived CO₂-are recalculated. bc) Benthic δ¹⁸O global compilation (Westerhold et al., 2020). ed)
Schematic representation of main paleoceanographic and paleogeographic changes over the studied time interval for the Northern and Southern Hemisphere. ACC arrow refers to a shallow circulation not synonymous with the deep late Miocene ACC described by Evangelinos et al. (2024) ACC: Yellow and blue vertical bands show main warming and cold periods as Middle Miocene Climatic Optimum (MMCO), Mi-1 glaciation, Late Oligocene Warming (LOW) and Middle Oligocene Glacial Interval (MOGI).

550 Antarctic Circumpolar Current. NCW: Northern Component Water.

560

565

570

575

580

585

The late Oligocene climate and CO_2 paradox has been discussed based on previously published lower resolution ϵ_p record from Site 925 (O'Brien et al., 2020). Our new results from two additional sites confirm the steep CO_2 decline through the late Oligocene warming and underscore the paradox. On a global scale, biomarker SST estimates do not show evidence for systematic cooling during the CO_2 decline (Guitián et al., 2019; Liu et al., 2018; O'Brien et al., 2020). If the interpretation of ϵ_p as a CO_2 decline is correct, it suggests that climate sensitivity was either significantly weaker so that no appreciable change in global mean surface temperature occurred, or that available paleotemperature estimates reflect a significant misinterpretation of measured biomarker signals. a very different set of feedbacks and climate sensitivity during this time, or widespread regional heat transport effects on regional temperatures or significant misinterpretation of measured biomarker temperature signals. During this time the inferred CO_2 decline also coincides with sequence stratigraphic evidence for ice margin retreat in Antarctica (Levy et al., 2019; Salabarnada et al., 2018), and sea level transgressions inferred from estimates of deep sea $\delta^{18}O_{sw}$ and Mg/Ca records (Miller et al., 2020), suggesting a substantially different relationship between ice expansion and CO_2 than characterized the late Neogene.

For the late Oligocene to early Miocene, the Southern Ocean Site 1168 is the only surface ocean temperature record which exhibits a long-term decline in SST coincident with the record of a large magnitude pCO_2 decline and decline in radiative forcing from the greenhouse effect. This long term cooling is despite the equatorward drift of the site over this time interval (Guitián and Stoll, 2021). Potentially, If the ODP Site 1168 temperature trend reflects is more representative of global average temperature during the CO_2 decline trends, and whereas the long term alkenone temperature record at Newfoundland Ridge Site 1406 and Site 1404 (Liu et al. 2018) is affected dominated by variations in the heat transport from the Gulf Stream, that then the 1168 temperature trend may reflect overwhelms the signal of radiative greenhouse forcing. While there is no evidence of a concomitant long term cooling in the benthic $\delta^{18}O$ series (e.g. Westerhold et al. (2020)), the ε_p minimum at 19 Ma coincides with a local maximum in benthic $\delta^{18}O$.

A decoupling was at one time proposed for the late Miocene based on apparent negligible pCO₂ change and substantial cooling of SST (LaRiviere et al., 2012). Revisions of the alkenone carbon fractionation to CO₂ calibration approaches for low pCO₂ periods have refined the record from the last 15 Ma, revealing clear pCO₂-SST covariation (Rae et al., 2021; Stoll et al., 2019). However, the Oligocene paradox is not easily resolvable from updated calibration of the ε_p -CO₂ relationship.__because thThe late Oligocene divergenceparadox arises from an inverse correlation between ε_p and SST reconstructions- in regions other than the Southern Ocean such as the North Atlantic, and a lack of correlation between ε_p and the global climate signal in benthic δ^{18} O trends. The discrepancies between alkenone and published TEX86 at ODP 1168 suggests continued reevaluation of SST proxy interpretation are needed, along with evaluation of the potential influence of changing surface ocean circulation on SST in some locations such as the North Atlantic. Additionally, the divergence of CO₂ trends among ε_p and boron isotopes suggest that further interrogation of ocean chemistry and biogeochemical cycles potentially affecting the growth and physiology of alkenone producers and the calculation of CO₂ from boron isotopes, are crucial to reconcile climate sensitivity to CO₂ in the Oligocene to early Miocene. Therefore, continued re evaluation of SST records and interrogation of biogeochemical cycles potentially affecting the growth and physiology of alkenone producers, are needed to reconcile climate sensitivity to CO₂ in the Oligocene to early Miocene.

5 Conclusions

590

595

600

605

The new long term alkenone ε_p records from the Oligocene to early Miocene at North Atlantic Site IODP 1406 and Southern Ocean Site ODP 1168 reveal a significant 8 to 10 ‰ shift. The <u>highest resolution Site 1406 new</u>-records resolve <u>an</u> abrupt 3 ‰ declines from 27 to 24.5 Ma and 24 to 22.5 Ma. The long term trend is comparable with previous lower resolution analysis when they are recalculated with the same methodology.

In addition to CO_2 , ε_p may be modified by changes in cellular surface area to volume ratio and growth rate regulated by light, temperature and nutrients. However, our assessment of these effects using records of coccolith size and alkenone temperature estimates for exact time intervals of ε_p determination, shows that size and temperature-stimulated growth rate effects have a negligible impact in the long term declining trend. The similarity of ε_p in widely separated sites experiencing contrasting temperature histories strongly suggests a global CO_2 decline as the most likely cause of the declining ε_p . At the same time, our high-resolution sampling reveals significant orbital scale variability in ε_p and underscores the potential for aliasing in low resolution records. Higher resolution ε_p time series, and more precise age models on legacy ε_p records to facilitate more confident comparisons of trends among sites, will provide a better characterization of the key long term trends.

Our results highlight the paradox of complex relationships between CO_2 indicators and SST at both the orbital and multimillion year timescales. The higher resolution sampling between 2829.7 to 289.7 Ma shows that orbital ϵ_p maxima do not coincide with orbital minima in ice volume and/or warmer deep ocean temperature. Similarly, through the late Oligocene warming, CO_2 decline contrasts with evidence for Antarctic ice retreat and evidence of stable or warming SST. The transition from late Oligocene to early Miocene, reaching minimum CO_2 around 19 Ma, is coincident with significant cooling only in the Southern Ocean Site 1168, but not the North Atlantic site which may be more affected by changes in ocean heat transport.

Data availability

Data presented in this paper is stored at Zenodo public repository (https://doi.org/10.5281/zenodo.13908062)

610 Author contribution

Study was conceived by HMS and PJP. Analysis completed by JG, SRP, RSW and LA. Interpretation by JG and HMS. Writing of original draft by JG and HMS with support of PJP.

Competing interests

The contact author has declared that none of the authors has any competing interests.

615 Acknowledgments

This paper presents data on sediment samples provided by the Ocean Drilling Program (ODP, IODP). We thank Maddie Santos for lab assistance with biogenic Si determinations. We thank Madalina Jaggi for assistance with carbonate stable isotope measurements.

Financial support

620 This research was funded by the Swiss National Science FoundationAward 200021_182070 to HMS.

References

- Auderset, A., Moretti, S., Taphorn, B., Ebner, P.-R., Kast, E., Wang, X.T., Schiebel, R., Sigman, D.M., Haug, G.H., Martínez-García, A., 2022. Enhanced ocean oxygenation during Cenozoic warm periods. Nature 609, 77-82.
- Baczynski, A.A., Polissar, P.J., Juchelka, D., Schwieters, J., Hilkert, A., Summons, R.E., Freeman, K.H., 2018. Picomolar-scale compound-specific isotope analyses. Rapid Communications in Mass Spectrometry 32, 730-738.
- Behrenfeld, M.J., Boss, E., Siegel, D.A., Shea, D.M., 2005. Carbon-based ocean productivity and phytoplankton physiology from space. Global biogeochemical cycles 19.
 - Blaauw, M., Christen, J.A., 2011. Flexible paleoclimate age-depth models using an autoregressive gamma process. Bayesian analysis 6, 457-474.
- Boller, A.J., Thomas, P.J., Cavanaugh, C.M., Scott, K.M., 2011. Low stable carbon isotope fractionation by coccolithophore RubisCO. Geochimica et cosmochimica acta 75, 7200-7207.
 - Bolton, C.T., Hernandez-Sanchez, M.T., Fuertes, M.A., Gonzalez-Lemos, S., Abrevaya, L., Mendez-Vicente, A., Flores, J.A., Probert, I., Giosan, L., Johnson, J., Stoll, H.M., 2016. Decrease in coccolithophore calcification and CO2 since the middle Miocene. Nat Commun 7, 10284.
- Bolton, C.T., Stoll, H.M., 2013. Late Miocene threshold response of marine algae to carbon dioxide limitation. Nature 500, 558-562.
 - Bradshaw, C.D., Langebroek, P.M., Lear, C.H., Lunt, D.J., Coxall, H.K., Sosdian, S.M., de Boer, A.M., 2021. Hydrological impact of Middle Miocene Antarctic ice-free areas coupled to deep ocean temperatures. Nature Geoscience 14, 429-436.
 - Breitenbach, S.F., Bernasconi, S.M., 2011. Carbon and oxygen isotope analysis of small carbonate samples (20 to 100 μg)
- with a GasBench II preparation device. Rapid Communications in Mass Spectrometry 25, 1910-1914.
 Consortium, C.P., 2023. Toward a Cenozoic history of atmospheric CO₂. Science 382, eadi5177.
 Cramer, B., Miller, K., Barrett, P., Wright, J., 2011. Late Cretaceous–Neogene trends in deep ocean temperature and continental ice volume: Reconciling records of benthic foraminiferal geochemistry (δ18O and Mg/Ca) with sea level history. Journal of Geophysical Research: Oceans 116.
- 645 Curry, W., Shackleton, N., Richter, C., 1995. Leg 154. Synthesis. Proceedings ODP, Initial Reports 154, 421-442. Deconto, R.M., Pollard, D., Wilson, P.A., Palike, H., Lear, C.H., Pagani, M., 2008. Thresholds for Cenozoic bipolar glaciation. Nature 455, 652-656.
 - Erdei, B., Utescher, T., Hably, L., Tamas, J., Roth-Nebelsick, A., Grein, M., 2012. Early Oligocene continental climate of the Palaeogene Basin (Hungary and Slovenia) and the surrounding area. Turkish Journal of Earth Sciences 21, 153-186.
- Evangelinos, D., Etourneau, J., van de Flierdt, T., Crosta, X., Jeandel, C., Flores, J.-A., Harwood, D.M., Valero, L., Ducassou, E., Sauermilch, I., 2024. Late Miocene onset of the modern Antarctic circumpolar current. Nature Geoscience 17, 165-170. Evans, D., Brugger, J., Inglis, G.N., Valdes, P., 2024. The Temperature of the Deep Ocean Is a Robust Proxy for Global Mean Surface Temperature During the Cenozoic. Paleoceanography and Paleoclimatology 39, e2023PA004788.
 - Exon, N., Kennett, J., Malone, M., 2001. 1. LEG 189 SUMMARY, Proceedings of the Ocean Drilling Program.
- Fielding, S.R., 2013. Emiliania huxleyi specific growth rate dependence on temperature. Limnology and Oceanography 58, 663-666.
 - Foster, G.L., Royer, D.L., Lunt, D.J., 2017. Future climate forcing potentially without precedent in the last 420 million years. Nature Communications 8, 14845.
- Freeman, K.H., Hayes, J., 1992. Fractionation of carbon isotopes by phytoplankton and estimates of ancient CO2 levels. Global Biogeochemical Cycles 6, 185-198.
 - Golledge, N.R., 2020. Long-term projections of sea-level rise from ice sheets. Wiley Interdisciplinary Reviews: Climate Change 11, e634.
 - González-Lanchas, A., Hernández-Alméida, I., Flores, J.A., Sierro, F.J., Guitian, J., Stoll, H.M., 2021. Carbon Isotopic Fractionation of Alkenones and Gephyrocapsa Coccoliths Over the Late Quaternary (Marine Isotope Stages 12–9) Glacial-
- Interglacial Cycles at the Western Tropical Atlantic. Paleoceanography and Paleoclimatology 36, e2020PA004175.
 - Gradstein, F.M., Ogg, J.G., Schmitz, M., Ogg, G., 2012. The geologic time scale 2012. elsevier.
 - Greenop, R., Sosdian, S.M., Henehan, M.J., Wilson, P.A., Lear, C.H., Foster, G.L., 2019. Orbital forcing, ice-volume and CO2 across the Oligocene-Miocene Transition. Paleoceanography and Paleoclimatology.
- Guitián, J., Dunkley Jones, T., Hernández-Almeida, I., Löffel, T., Stoll, H.M., 2020. Adaptations of coccolithophore size to selective pressures during the Oligocene to Early Miocene high CO2 world. Paleoceanography and Paleoclimatology 35, e2020PA003918.
 - Guitián, J., Phelps, S., Polissar, P.J., Ausín, B., Eglinton, T.I., Stoll, H.M., 2019. Midlatitude Temperature Variations in the Oligocene to Early Miocene. Paleoceanography and Paleoclimatology 34, 1328-1343.
 - Guitián, J., Stoll, H.M., 2021. Evolution of Sea Surface Temperature in the Southern Mid-latitudes from Late Oligocene through Early Miocene. Paleoceanography and Paleoclimatology 36, e2020PA004199.
- Hansen, J., Sato, M., Russell, G., Kharecha, P., 2013. Climate sensitivity, sea level and atmospheric carbon dioxide. Philosophical Transactions of the Royal Society A: Mathematical, Physical and Engineering Sciences 371, 20120294. Hay, W.W., DeConto, R.M., Wold, C.N., Wilson, K.M., Voigt, S., Schulz, M., Wold, A.R., Dullo, W.-C., Ronov, A.B.,
- Balukhovsky, A.N., 1999. Alternative global Cretaceous paleogeography.
 Henderiks, J., Pagani, M., 2007. Refining ancient carbon dioxide estimates: Significance of coccolithophore cell size for alkenone-based pCO2 records. Paleoceanography 22.
 - Henderiks, J., Pagani, M., 2008. Coccolithophore cell size and the Paleogene decline in atmospheric CO2. Earth and planetary science letters 269, 576-584.

- Hernández-Almeida, I., Guitián, J., Tanner, T., Zhang, H., Stoll, H.M., 2023. Hydrographic control on carbon isotope fractionation in coccolithophores in the North Atlantic during the Mid-Pleistocene. Quaternary Science Reviews 309, 108081. Hernández-Almeida, I., Krumhardt, K.M., Zhang, H., Stoll, H.M., 2020. Estimation of physiological factors controlling carbon isotope fractionation in coccolithophores in photic zone and core-top samples. Geochemistry, Geophysics, Geosystems 21, e2020GC009272.
- Hou, S., Lamprou, F., Hoem, F.S., Hadju, M.R.N., Sangiorgi, F., Peterse, F., Bijl, P.K., 2023a. Lipid-biomarker-based sea surface temperature record offshore Tasmania over the last 23 million years. Climate of the Past 19, 787-802.
 - Hou, S., Stap, L.B., Paul, R., Nelissen, M., Hoem, F.S., Ziegler, M., Sluijs, A., Sangiorgi, F., Bijl, P.K., 2023b. Reconciling Southern Ocean fronts equatorward migration with minor Antarctic ice volume change during Miocene cooling. Nature Communications 14, 7230.
- Jasper, J.P., Hayes, J., 1994. Reconstruction of Paleoceanic PCO 2 levels from carbon isotopic compositions of sedimentary biogenic components, Carbon Cycling in the Glacial Ocean: Constraints on the Ocean's Role in Global Change. Springer, pp. 323-341.
 - Krumhardt, K.M., Lovenduski, N.S., Iglesias-Rodriguez, M.D., Kleypas, J.A., 2017. Coccolithophore growth and calcification in a changing ocean. Progress in oceanography 159, 276-295.
- LaRiviere, J.P., Ravelo, A.C., Crimmins, A., Dekens, P.S., Ford, H.L., Lyle, M., Wara, M.W., 2012. Late Miocene decoupling of oceanic warmth and atmospheric carbon dioxide forcing. Nature 486, 97-100.
 - Lear, C.H., Elderfield, H., Wilson, P., 2000. Cenozoic deep-sea temperatures and global ice volumes from Mg/Ca in benthic foraminiferal calcite. science 287, 269-272.
 - Lear, C.H., Rosenthal, Y., Coxall, H.K., Wilson, P., 2004. Late Eocene to early Miocene ice sheet dynamics and the global carbon cycle. Paleoceanography 19.
- Levy, R., Meyers, S., Naish, T., Golledge, N., McKay, R., Crampton, J., DeConto, R., De Santis, L., Florindo, F., Gasson, E., 2019. Antarctic ice-sheet sensitivity to obliquity forcing enhanced through ocean connections. Nature Geoscience, 1. Liang, J.-Q., Leng, Q., Höfig, D.F., Niu, G., Wang, L., Royer, D.L., Burke, K., Xiao, L., Zhang, Y.G., Yang, H., 2022a. Constraining conifer physiological parameters in leaf gas-exchange models for ancient CO2 reconstruction. Global and Planetary Change 209, 103737.
- Liang, J.-q., Leng, Q., Xiao, L., Höfig, D.F., Royer, D.L., Zhang, Y.G., Yang, H., 2022b. Early Miocene redwood fossils from Inner Mongolia: CO2 reconstructions and paleoclimate effects of a low Mongolian plateau. Review of Palaeobotany and Palynology 305, 104743.
 - Liebrand, D., de Bakker, A.T., Beddow, H.M., Wilson, P.A., Bohaty, S.M., Ruessink, G., Palike, H., Batenburg, S.J., Hilgen, F.J., Hodell, D.A., Huck, C.E., Kroon, D., Raffi, I., Saes, M.J., van Dijk, A.E., Lourens, L.J., 2017. Evolution of the early
- Antarctic ice ages. Proc Natl Acad Sci U S A 114, 3867-3872. Lisiecki, L.E., Raymo, M.E., 2005. A Pliocene-Pleistocene stack of 57 globally distributed benthic δ18O records. Paleoceanography 20.
 - Liu, Z., He, Y., Jiang, Y., Wang, H., Liu, W., Bohaty, S.M., Wilson, P.A., 2018. Transient temperature asymmetry between hemispheres in the Palaeogene Atlantic Ocean. Nature Geoscience 11, 656.
- Liu, Z., Pagani, M., Zinniker, D., Deconto, R., Huber, M., Brinkhuis, H., Shah, S.R., Leckie, R.M., Pearson, A., 2009. Global cooling during the eocene-oligocene climate transition. Science 323, 1187-1190.
 Londoño, L., Royer, D.L., Jaramillo, C., Escobar, J., Foster, D.A., Cárdenas-Rozo, A.L., Wood, A., 2018. Early Miocene CO 2 estimates from a Neotropical fossil leaf assemblage exceed 400 ppm. American Journal of Botany 105, 1929-1937.
 - Miller, K.G., Browning, J.V., Schmelz, W.J., Kopp, R.E., Mountain, G.S., Wright, J.D., 2020. Cenozoic sea-level and
- cryospheric evolution from deep-sea geochemical and continental margin records. Science advances 6, eaaz1346.
 Miller, K.G., Wright, J.D., Fairbanks, R.G., 1991. Unlocking the ice house: Oligocene-Miocene oxygen isotopes, eustasy, and margin erosion. Journal of Geophysical Research: Solid Earth 96, 6829-6848.
 - Misra, S., Froelich, P.N., 2012. Lithium isotope history of Cenozoic seawater: changes in silicate weathering and reverse weathering. Science 335, 818-823.
- Mook, W., Bommerson, J., Staverman, W., 1974. Carbon isotope fractionation between dissolved bicarbonate and gaseous carbon dioxide. Earth and Planetary science letters 22, 169-176.

 Moraweck, K., Grein, M., Konrad, W., Kvaček, J., Kova-Eder, J., Neinhuis, C., Traiser, C., Kunzmann, L., 2019. Leaf traits
 - of long-ranging Paleogene species and their relationship with depositional facies, climate and atmospheric CO2 level; Leaf traits of long-ranging Paleogene species and their relationship with depositional facies, climate and atmospheric CO2 level. Palaeontographica Abteilung B: Palaeophytologie 298, 93-172.
- Novak, J., McGrath, S.M., Wang, K.J., Liao, S., Clemens, S.C., Kuhnt, W., Huang, Y., 2022. U38MEK' Expands the linear dynamic range of the alkenone sea surface temperature proxy. Geochimica et Cosmochimica Acta 328, 207-220.
 - O'Brien, C.L., Huber, M., Thomas, E., Pagani, M., Super, J.R., Elder, L.E., Hull, P.M., 2020. The enigma of Oligocene climate and global surface temperature evolution. Proceedings of the National Academy of Sciences 117, 25302-25309.
- Pagani, M., Arthur, M.A., Freeman, K.H., 1999. Miocene evolution of atmospheric carbon dioxide. Paleoceanography 14, 273-292.
 - Pagani, M., Arthur, M.A., Freeman, K.H., 2000. Variations in Miocene phytoplankton growth rates in the southwest Atlantic: Evidence for changes in ocean circulation. Paleoceanography 15, 486-496.
 - Pagani, M., Holland, H., Turekian, K., 2014. 12.13 Biomarker-based inferences of past climate: The alkenone pCO2 proxy.
- Treatise on Geochemistry, edited by: Holland, HD and Turekian, KK, Elsevier, Oxford, 361-378.

 Pagani, M., Huber, M., Liu, Z., Bohaty, S.M., Henderiks, J., Sijp, W., Krishnan, S., DeConto, R.M., 2011. The role of carbon dioxide during the onset of Antarctic glaciation. science 334, 1261-1264.

- Pagani, M., Zachos, J.C., Freeman, K.H., Tipple, B., Bohaty, S., 2005. Marked decline in atmospheric carbon dioxide concentrations during the Paleogene. Science 309, 600-603.
- Pfuhl, H.A., McCave, I.N., 2003. Integrated age models for the early Oligocene-early Miocene, sites 1168 and 1170–1172, Proc. ODP, Sci. Results, pp. 1-21.
 - Popp, B.N., Kenig, F., Wakeham, S.G., Laws, E.A., Bidigare, R.R., 1998. Does growth rate affect ketone unsaturation and intracellular carbon isotopic variability in Emiliania huxleyi? Paleoceanography 13, 35-41.
- Rae, J.W., Zhang, Y.G., Liu, X., Foster, G.L., Stoll, H.M., Whiteford, R.D., 2021. Atmospheric CO2 over the past 66 million years from marine archives. Annual Review of Earth and Planetary Sciences 49, 609-641.
- Ragueneau, O., Tréguer, P., Leynaert, A., Anderson, R., Brzezinski, M., DeMaster, D., Dugdale, R., Dymond, J., Fischer, G., Francois, R., 2000. A review of the Si cycle in the modern ocean: recent progress and missing gaps in the application of biogenic opal as a paleoproductivity proxy. Global and Planetary Change 26, 317-365.
- Rama-Corredor, O., Cortina, A., Martrat, B., Lopez, J.F., Grimalt, J.O., 2018. Removal of bias in C37 alkenone-based sea surface temperature measurements by high-performance liquid chromatography fractionation. Journal of Chromatography A 1567, 90-98.
 - Rau, G.H., Riebesell, U., Wolf-Gladrow, D., 1996. A model of photosynthetic 13C fractionation by marine phytoplankton based on diffusive molecular CO2 uptake. Marine Ecology Progress Series 133, 275-285.
 - Raymo, M.E., Ruddiman, W.F., 1992. Tectonic forcing of late Cenozoic climate. Nature 359, 117-122.
- Reichgelt, T., D'Andrea, W.J., Valdivia-McCarthy, A.d.C., Fox, B.R., Bannister, J.M., Conran, J.G., Lee, W.G., Lee, D.E., 2020. Elevated CO 2, increased leaf-level productivity, and water-use efficiency during the early Miocene. Climate of the Past 16, 1509-1521.
 - Reilly, T.J., Miller, K.G., Feigenson, M.D., 2002. Latest Eocene-earliest Miocene Sr isotopic reference section, Site 522, eastern South Atlantic. Paleoceanography 17, 18-11-18-19.
- Roth-Nebelsick, A., Oehm, C., Grein, M., Utescher, T., Kunzmann, L., Friedrich, J.-P., Konrad, W., 2014. Stomatal density and index data of Platanus neptuni leaf fossils and their evaluation as a CO2 proxy for the Oligocene. Review of Palaeobotany and Palynology 206, 1-9.
 - Rugenstein, J.K.C., Ibarra, D.E., von Blanckenburg, F., 2019. Neogene cooling driven by land surface reactivity rather than increased weathering fluxes. Nature 571, 99-102.
- Salabarnada, A., Escutia, C., Röhl, U., Nelson, C.H., McKay, R., Jiménez-Espejo, F., Bijl, P., Hartman, J., Strother, S., Salzmann, U., 2018. Paleoceanography and ice sheet variability offshore Wilkes Land, Antarctica—Part 1: Insights from late Oligocene astronomically paced contourite sedimentation. Climate of the Past 14, 991-1014.
 - Shackleton, N., 1987. Oxygen isotopes, ice volume and sea level. Quaternary science reviews 6, 183-190.

780

- Sherman, E., Moore, J.K., Primeau, F., Tanouye, D., 2016. Temperature influence on phytoplankton community growth rates. Global Biogeochemical Cycles 30, 550-559.
- Sosdian, S.M., Greenop, R., Hain, M., Foster, G.L., Pearson, P.N., Lear, C.H., 2018. Constraining the evolution of Neogene ocean carbonate chemistry using the boron isotope pH proxy. Earth and Planetary Science Letters 498, 362-376.
- Steinthorsdottir, M., Jardine, P.E., Rember, W.C., 2021. Near-future pCO2 during the hot Mid Miocene Climatic Optimum. Paleoceanography and Paleoclimatology 36.
- Stoll, H.M., Guitian, J., Hernandez-Almeida, I., Mejia, L.M., Phelps, S., Polissar, P., Rosenthal, Y., Zhang, H., Ziveri, P., 2019. Upregulation of phytoplankton carbon concentrating mechanisms during low CO2 glacial periods and implications for the phytoplankton pCO2 proxy. Quaternary Science Reviews 208, 1-20.
- Stoll, H.M., Pena, L.D., Hernandez-Almeida, I., Guitián, J., Tanner, T., Pälike, H., 2024. Nonlinear increase in seawater 87Sr &fsr in the Oligocene to early Miocene and implications for climate-sensitive weathering. Clim. Past 20, 25-36.
 - Sun, B.-N., Wang, Q.-J., Konrad, W., Ma, F.-J., Dong, J.-L., Wang, Z.-X., 2017. Reconstruction of atmospheric CO2 during the Oligocene based on leaf fossils from the Ningming Formation in Guangxi, China. Palaeogeography, Palaeoclimatology, Palaeoecology 467, 5-15.
- Super, J.R., Thomas, E., Pagani, M., Huber, M., O'Brien, C., Hull, P.M., 2018. North Atlantic temperature and p CO2 coupling in the early-middle Miocene. Geology 46, 519-522.
- Sutton, R.T., Dong, B., Gregory, J.M., 2007. Land/sea warming ratio in response to climate change: IPCC AR4 model results and comparison with observations. Geophysical research letters 34.
 - Tanner, T., Hernández-Almeida, I., Drury, A.J., Guitián, J., Stoll, H., 2020. Decreasing atmospheric CO2 during the late Miocene cooling. Paleoceanography and Paleoclimatology 35, e2020PA003925.
- Tesfamichael, T., Jacobs, B., Tabor, N., Michel, L., Currano, E., Feseha, M., Barclay, R., Kappelman, J., Schmitz, M., 2017. Settling the issue of "decoupling" between atmospheric carbon dioxide and global temperature:[CO2] atm reconstructions across the warming Paleogene-Neogene divide. Geology 45, 999-1002.
 - Tierney, J.E., Tingley, M.P., 2015. A TEX(8)(6) surface sediment database and extended Bayesian calibration. Sci Data 2, 150029.
- Tierney, J.E., Tingley, M.P., 2018. BAYSPLINE: A new calibration for the alkenone paleothermometer. Paleoceanography and Paleoclimatology 33, 281-301.
 - Torres Romero, I., Clark, A.J., Wijker, R.S., Jaggi, M., Zhang, H., Stoll, H.M., 2024. Temperature-dependent carbon isotope fractionation in coccolithophores. Frontiers in Earth Science 12, 1331179.
 - Torsvik, T.H., Van der Voo, R., Preeden, U., Mac Niocaill, C., Steinberger, B., Doubrovine, P.V., Van Hinsbergen, D.J.,
- Domeier, M., Gaina, C., Tohver, E., 2012. Phanerozoic polar wander, palaeogeography and dynamics. Earth-Science Reviews 114, 325-368.

- van Hinsbergen, D.J., de Groot, L.V., van Schaik, S.J., Spakman, W., Bijl, P.K., Sluijs, A., Langereis, C.G., Brinkhuis, H., 2015. A paleolatitude calculator for paleoclimate studies. PloS one 10.
- Van Peer, T.E., Xuan, C., Lippert, P.C., Liebrand, D., Agnini, C., Wilson, P.A., 2017. Extracting a detailed 815 magnetostratigraphy from weakly magnetized, Oligocene to early Miocene sediment drifts recovered at IODP Site U1406 (Newfoundland margin, northwest Atlantic Ocean). Geochemistry, Geophysics, Geosystems 18, 3910-3928. Westerhold, T., Marwan, N., Drury, A.J., Liebrand, D., Agnini, C., Anagnostou, E., Barnet, J.S., Bohaty, S.M., De

Vleeschouwer, D., Florindo, F., 2020. An astronomically dated record of Earth's climate and its predictability over the last 66

million years. Science 369, 1383-1387.

- 820 Wilkes, E.B., Lee, R.B., McClelland, H.L., Rickaby, R.E., Pearson, A., 2018. Carbon isotope ratios of coccolith-associated polysaccharides of Emiliania huxleyi as a function of growth rate and CO2 concentration. Organic geochemistry 119, 1-10. Zachos, J., Pagani, M., Sloan, L., Thomas, E., Billups, K., 2001. Trends, rhythms, and aberrations in global climate 65 Ma to present. Science 292, 686-693.
- Zachos, J.C., Dickens, G.R., Zeebe, R.E., 2008. An early Cenozoic perspective on greenhouse warming and carbon-cycle 825 dynamics. Nature 451, 279-283.
 - Zhang, Y.G., Pagani, M., Liu, Z., Bohaty, S.M., Deconto, R., 2013. A 40-million-year history of atmospheric CO(2). Philos Trans A Math Phys Eng Sci 371, 20130096.